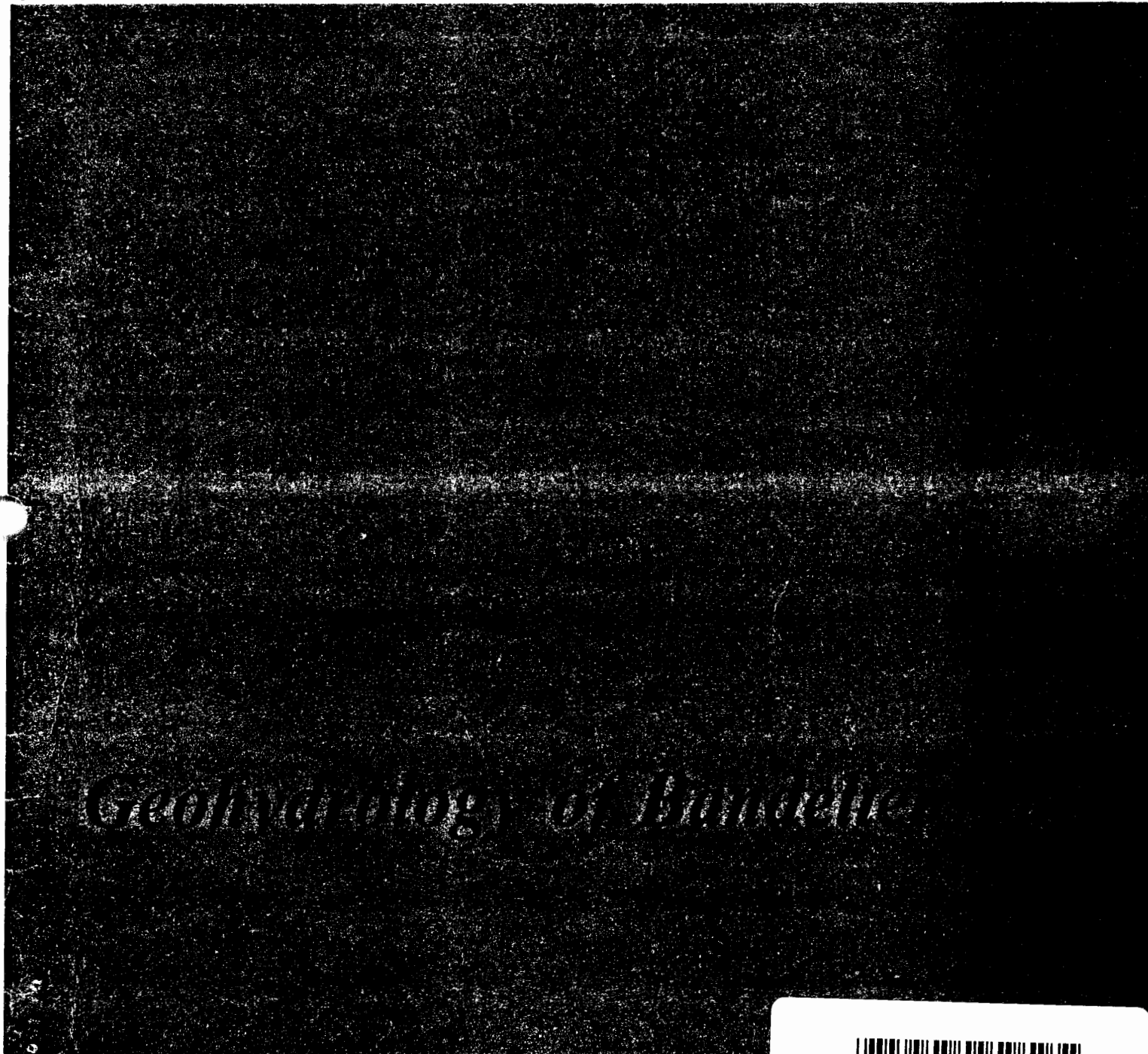


LA-8962-MS

ER Record I.D.# 0006273

Los Alamos National Laboratory is operated by the University of California for the United States Department of Energy under contract W-7405-ENG-36.



*Geochronology of Basalts*



10400

**Los Alamos** Los Alamos National Laboratory  
Los Alamos, New Mexico 87545

LA-8962-MS

UC-11

Issued: October 1981

## **Geohydrology of Bandelier Tuff**

W. V. Abeele  
M. L. Wheeler  
B. W. Burton

**Los Alamos** Los Alamos National Laboratory  
Los Alamos, New Mexico 87545

## CONTENTS

ABSTRACT	1
I. INTRODUCTION	1
II. PHYSICAL SETTING	3
A. Geology of the Los Alamos Area	3
B. Tuff Structure and Texture	6
C. General Climatology	6
D. Precipitation	7
1. Recent Climatic Records	7
2. Tree-Ring Evidence	8
III. SURFACE WATER	9
IV. SATURATED FLOW	11
V. GAUGING STATION, AREA G	12
A. Introduction	12
B. Location and Watershed Area	12
C. Weir and Stilling Basin	12
D. Runoff Events	14
E. Weir Calibration	14
1. Theoretical	14
2. Empirical	15
F. Rainfall-Runoff Calibration	15
VI. SATURATED AND UNSATURATED HYDRAULIC CONDUCTIVITIES	16
A. General	16
B. Crushed Tuff	17
1. Measurements	17
2. Predictive Methods	19
C. Solid Tuff	21
1. Measurements	21
2. Predictive Methods	21
VII. HYDROLOGIC MONITORING	22
A. Parameters Influencing Neutron Probe Readings	22
B. Prior Measurements	22
C. Current Monitoring	25
1. History	25
2. Data Discussion	25
a. Area C	25
b. Area G	27
c. Area F	29
d. TA-51	30
3. Geophysical Logging	30
4. Justification for Converting to "Inactive"	30

VIII. TRITIUM MIGRATION . . . . .	31
A. Tritiated Water in Soils . . . . .	31
B. Emanation of Tritiated Water . . . . .	33
IX. STRATIGRAPHIC CONTROLS ON FLOW . . . . .	37
X. RADIONUCLIDE TRANSPORT STUDIES . . . . .	38
A. Downward Migration through Leaching . . . . .	38
B. Upward Migration via Evapotranspiration . . . . .	38
XI. SHEAR IN WET COHESIONLESS SOILS AND CRUSHED TUFF . . . . .	39
ACKNOWLEDGMENTS . . . . .	43
REFERENCES . . . . .	43

APPENDIX

SUMMARY OF DEPTH RANGES AND MEASUREMENT DATES FOR MONITORING HOLES . . . . .	46
---	----

FIGURES

1 Burial site map . . . . .	2
2 Geologic stratigraphic relationships of Los Alamos County from Sierra de los Valles to the Rio Grande . . . . .	3
3 Base map . . . . .	10
4 Location of watershed and stilling basin, Area G, TA-54 . . . . .	13
5 Cross-section of stilling basin . . . . .	13
6 Weir plate details . . . . .	13
7 Precipitation and runoff, Area G weir . . . . .	14
8 Calculated hydraulic conductivities compared with measured data . . . . .	20
9 Saturation ratio as a function of matric potential (moisture characteristic curves) . . . . .	22
10 Hydraulic conductivity as a function of matric potential . . . . .	23
11 Hydraulic conductivity as a function of saturation ratio . . . . .	23
12 Moisture distributions at TA-49 (Abrahams, Weir, & Purtymun, 1961) . . . . .	24
13 Moisture distributions in Bandelier Tuff near TA-21 (Purtymun & Kennedy, 1966). . . . .	25
14 Moisture Hole CP2-1 . . . . .	26
15 Moisture Hole CP6-1 . . . . .	27
16 Moisture Hole GP1-1 . . . . .	28
17 Moisture Hole GS50-3 . . . . .	28
18 Moisture Hole GS50-5 . . . . .	29
19 Moisture Hole GP7-2 . . . . .	30
20 Resistance tests on tuff . . . . .	40
21 Resistance tests on soil . . . . .	41

## TABLES

I	PROPERTIES OF TUFF AS A FUNCTION OF DEGREE OF WELDING . . . . .	5
II	UPDATED PRECIPITATION WITH PROBABILITY LEVELS EQUAL TO OR LESS THAN (mm of ppt) . . . . .	8
III	DISCHARGE DATA FOR AREA G WEIR . . . . .	15
IV	PRECIPITATION AND RUNOFF ON JULY 10, 1980 . . . . .	16
V	HYDRAULIC CHARACTERISTICS OF CRUSHED BANDELIER TUFF AS A FUNCTION OF MATRIC POTENTIAL . . . . .	18
VI	HYDRAULIC CONDUCTIVITY OF SOLID TUFF AS A FUNCTION OF MATRIC POTENTIAL . . . . .	21
VII	MOISTURE CONTENT OF BANDELIER TUFF . . . . .	24
VIII	HISTORY AND CURRENT STATUS AT MONITORING HOLES . . . . .	26
IX	DECREASE IN RADIOACTIVITY NEAR SHAFT 13 AS A FUNCTION OF DISTANCE FROM THE SHAFT ALONG A S-W AXIS . . . . .	32
X	DECREASE IN RADIOACTIVITY NEAR SHAFTS 50 AND 59 AS A FUNCTION OF DISTANCE FROM THE SHAFT . . . . .	33
XI	ACTIVITY AND FLUX OF TRITIATED WATER AT THE SOIL- ATMOSPHERE INTERFACE 4.7 m FROM THE CENTER OF GS-150 . . . . .	36
XII	VANE SHEAR TEST ON SOIL . . . . .	40
XIII	VANE SHEAR TEST ON CRUSHED TUFF . . . . .	40
XIV	RESISTANCE TO PENETRATION IN TUFF . . . . .	42
XV	RESISTANCE TO PENETRATION IN SOIL . . . . .	42
XVI	RESISTANCE TO PENETRATION IN TUFF AFTER PUDDLING . . . . .	43
XVII	RESISTANCE TO PENETRATION IN SOIL AFTER PUDDLING . . . . .	43

# GEOHYDROLOGY OF BANDELIER TUFF

by

W. V. Abeele  
M. L. Wheeler  
B. W. Burton

## ABSTRACT

The Los Alamos National Laboratory has been disposing of radioactive wastes since 1944. Environmental studies and monitoring for radioactive contamination started concurrently. In this report, only two mechanisms and rates by which the radionuclides can enter the environment are studied in detail: subsurface transport of radionuclides by migrating water, and diffusion of tritiated water (HTO) in the vapor phase. The report also includes a section concerning the influence of moisture on shear strength and possible resulting subsidences occurring in the pit overburdens. Because subsurface transport of radionuclides is influenced by the hydraulic conductivity and this in turn is regulated by the moisture content of any given material, a study was also undertaken involving precipitation, the most important climatic element influencing the geohydrology of any given area. Further work is in progress to correlate HTO emanation to atmospheric and pedological properties, especially including thermal characteristics of the tuff.

---

## I. INTRODUCTION

Wastes containing plutonium and other radionuclides have been buried at Los Alamos National Laboratory since the beginning of Laboratory operations in the early 1940s. Open pits or trenches have provided the principal disposal facility, but vertical shafts and covered seepage pits have been used for special waste forms. All shafts, pits, and trenches have been excavated in the surface of the Bandelier tuff, the principal rock-type exposed in the Los Alamos area (Fig. 1). The tuff (a nonwelded to welded volcanic ash) comprises an upland area called the Pajarito Plateau. The Plateau is dissected by numerous canyons trending east-west, all of which drain into the Rio Grande. Most of the Laboratory facilities, including the waste disposal sites, are located on the tops of the resulting finger-like mesas.

A large variety of waste types have been buried at Los Alamos National Laboratory. The bulk of the material is room-generated trash, such as paper, packing material, protective clothing, broken glassware, obsolete contaminated equipment, etc., which is generally contained in cardboard boxes or wooden crates. A wide variety of disposal operations are performed, ranging from shaft disposal of cylinders containing millicurie quantities of tritium to demolition and burial of entire contaminated buildings. During the Laboratory's early years, liquid wastes were disposed directly to the ground by discharging them into seepage pits. Since 1952, the sludges resulting from liquid waste treatment have been placed in drums for burial or mixed with cement and poured into shafts.

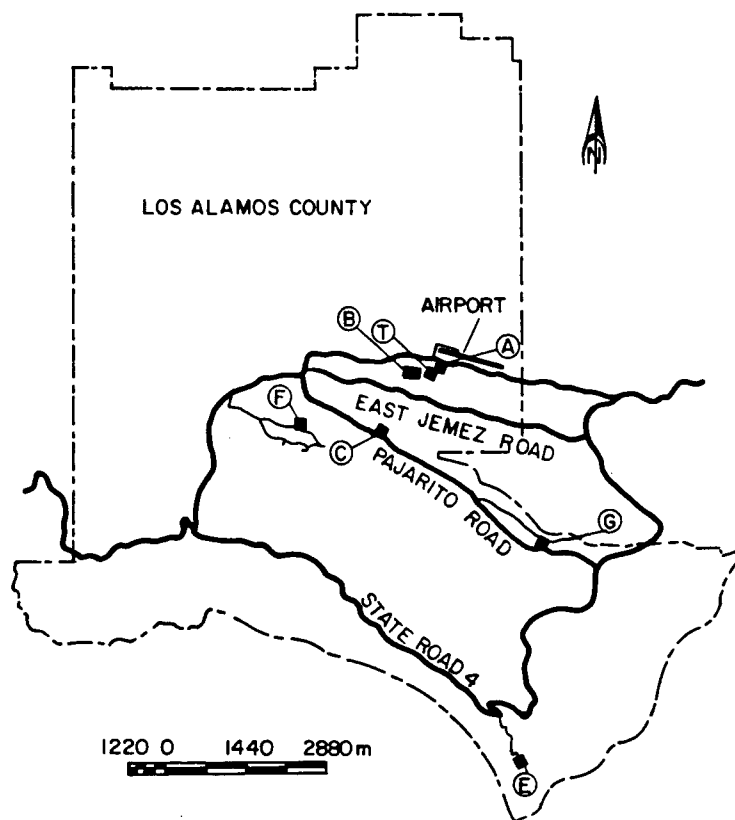


Fig. 1. Burial site map.

Presently, solid wastes are placed in open pits, characteristically about 10 m deep by 15 m wide by 130 m long. The wastes are placed in layers, with each layer covered with the crushed tuff excavated during construction of the pit. Location, physical description, and radionuclide content of the wastes are recorded in log books and on a computerized record keeping system. When a pit is filled to within approximately a meter of the ground surface, a cover of crushed tuff is overlaid and mounded about 1 m high to facilitate precipitation runoff. The surface is then reseeded with native vegetation for erosion control.

Present practices have evolved from a variety of burial procedures, but historically all practices are similar. Wastes are placed in trenches to within approximately a meter of the surface and the trench is then backfilled with uncontaminated crushed tuff. A records survey was made of the radionuclide content and composition of solid wastes disposed at Los Alamos National Laboratory since the beginning of the Laboratory (Rogers, 1977). Waste disposal records were highly variable in quality and quite incomplete until the mid-1950s. Detailed records of content and composition were not kept until 1959, and the quality of recording has improved steadily since that time. Guidelines for construction and use of solid waste disposal facilities at Area G, TA-54 have been in effect since 1956. The latest revision\* is consistent with established Department of Energy (DOE) Burial Site Criteria.

Determining the potential impact of buried radioactive wastes on the environment requires definition of the mechanisms and rates by which the radionuclides can enter the environment. The various

\*Memo H-7-80-660 To: Distribution (Operation Waste Management Committee), Through: Harry Jordan, H-DO; From: W. D. Purtymun, H-8, M. Wheeler, LS-6, and J. L. Warren, H-7 (December 10, 1980).

mechanisms can be divided into two major categories—natural phenomena more or less independent of human activity, and advertent acts by man, such as war, land excavation, sabotage, etc. All processes discussed here fall into the former category and can be further subdivided into two groups: chronic release processes, which occur at a more or less uniform rate when viewed on a time scale of tens to hundreds of years, and acute release processes consisting of single events separated by long periods of nonoccurrence. Chronic release mechanisms include exposure of the wastes by wind or water erosion, subsurface transport of radionuclides by migrating water, and plant or animal transfer of buried material to the surface.

This report is limited to the study of subsurface transport of radionuclides by migrating water or by diffusion of a radionuclide such as tritium in the vapor phase of tritiated water (HTO).

## II. PHYSICAL SETTING

### A. Geology of the Los Alamos Area

The volcanic and sedimentary rocks that occur in the Los Alamos area range in age from Miocene to Holocene. Rock types include sandstones and siltstones, crystalline rocks, and ash-flow tuffs (Fig. 2).

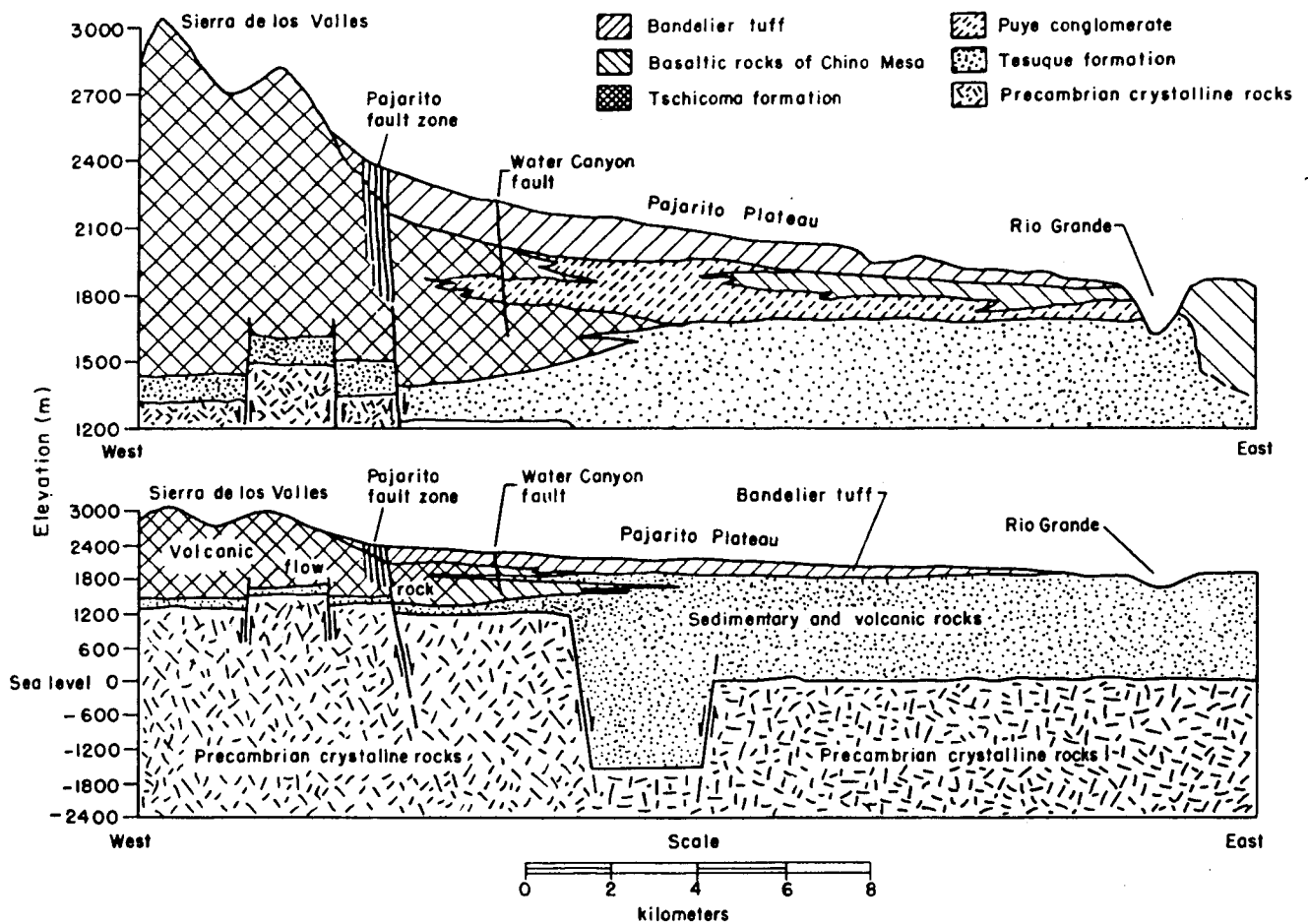


Fig. 2. Geologic stratigraphic relationships of Los Alamos County from Sierra de los Valles to the Rio Grande.

The oldest rock unit in the Los Alamos area is the Tesuque Formation, consisting of fossiliferous siltstones and sandstones with lenses of clay that were deposited as basin fill in the Rio Grande structural trough. Near Los Alamos these sediments are light pinkish-tan and include some interbedded basalts. The Tesuque underlies the Pajarito Plateau and is exposed at lower levels along the Puye Escarpment and in White Rock Canyon. The main water supply for Laboratory and domestic use is derived from the Tesuque. The age of the Tesuque is Miocene.

The Tschicoma Formation forms the major part of the interior mass of the central Jemez Mountains; thus, exposures are limited to the western and northern parts of the Los Alamos area. Rock types are porphyritic dacite, rhyodacite, and quartz latite containing phenocrysts of pyroxene, hornblende, biotite, plagioclase, and quartz (Bailey et al., 1969; Smith et al., 1970). Some units of latite and quartz latite in the Los Alamos area contain xenocrystic plagioclase that has been partially remelted, embayed, and resorbed, as well as subrounded and embayed quartz (Griggs, 1964). The maximum thickness of the 6.7 to 3.7 million-year-old (Myr) Tschicoma Formation exceeds 900 m (Bailey et al., 1969; Smith et al., 1970).

The Puye Formation, named for exposures in cliffs along the Puye Escarpment, is divided into two informal members, the lower Totavi Lentil, overlain by a fanglomerate. The basal Totavi Lentil (0 to 25 m thick) consists of well-rounded pebbles, cobbles, and small boulders of Precambrian quartzite and granite in a matrix of coarse arkosic sandstone. The upper unit is a poorly consolidated, silty, sandy conglomerate containing interlayered lapilli-tuff beds and volcanic mudflow deposits. The detritus is mostly dacite, rhyodacite, and quartz latite debris from erosion of the Tschicoma Formation (Bailey et al., 1979; Smith et al., 1970). The Puye is ~15 m thick in the eastern part of the Pajarito Plateau and thickens westward to ~220 m (Bailey et al., 1969). In the central and eastern parts of the plateau the Puye overlies the Tesuque Formation. It interfingers with basaltic andesite flows from the Cerros del Rio to the southeast and with younger flows of the Tschicoma to the west (DOE/EIS-0018, 1979).

The volcanic rocks of Cerros del Rio (Chino Mesa), which include some alkali olivine basalt, are mostly basaltic andesite flows and tuffs (0 to 460 m thick) containing xenocrysts of quartz (Smith et al., 1970). Some of these flows extend northwestward to form the steep walls of White Rock Canyon and cap high mesas to the east. Griggs (1964) mapped five units in the Los Alamos area. The volcanics of Cerros del Rio are less than 2.8 Myr old (Smith et al., 1970).

The basaltic andesite of Tank Nineteen (Smith et al., 1970) forms a broad shield volcano in the western part of the Cerros del Rio and ranges in thickness from 15 to 150 m. In the lower part of White Rock Canyon these flows overlie the Otowi Member of the Bandelier Tuff and tuffs of the Cerro Toledo Rhyolite.

Volcanism in the Jemez Mountains during the Pleistocene produced a series of rhyolite and quartz latite domes, ash flows, air-fall pumice, and obsidian. In the Los Alamos area these rocks are represented by the Cerro Toledo Rhyolite and the Bandelier Tuff.

The Cerro Toledo Rhyolite is a series of rhyolite domes, obsidian, tuffs, and tuff breccias that occur mostly within the Toledo Caldera (Smith et al., 1970). Exposures near Los Alamos occur in a small area in Rendija and Guaje Canyons. These reworked tuffs and sediments overlie the Puye Formation and are less than 30 m thick (DOE/EIS-0018, 1979).

The Bandelier Tuff is a sequence of nonwelded-to-welded rhyolite ash flows and pumice containing bi-pyramidal quartz and chatoyant sanidine (Smith et al., 1970). The tuff forms the upper parts of the Jemez Plateau on the western and the Pajarito Plateau on the eastern flanks of the Jemez Mountains. It is, therefore, the most important geologic unit at Los Alamos. All Laboratory facilities are constructed on the Bandelier Tuff. The formation is divided into two members, the lower Otowi and upper Tshirege, locally separated by tuffs of the Cerro Toledo Rhyolite. Each member is composed of a basal air-fall pumice overlain by a series of ash-flow units. The thickness of the tuff ranges from 10 to 320 m.

In the Los Alamos area the 1.4 Myr-old Otowi Member consists of a 0- to 10-m-thick basal bedded air-fall pumice (Guaje Pumice Bed) overlain by massive to poorly bedded nonwelded ash-flow deposits

containing abundant accidental lithic fragments. Ash flow units in the Otowi often easily erode to form characteristic pinnacle-shaped features. The thickness of this member in the Los Alamos area ranges from 0 to 80 m (DOE/EIS-0018, 1979).

The 1.1 Myr-old Tshirege Member consists of a 0.3-m-thick basal bedded air-fall pumice (Tsankawi Pumice Bed) overlain by nonwelded to welded ash flows containing genetically-related, hornblende-rich, quartz latite pumice and accidental lithic fragments (Bailey et al., 1969; Smith et al., 1970). The ash flows are often separated by pyroclastic surge deposits; pumice swarms occur intermittently. The Tshirege forms alternating vertical cliffs and steep slopes, caused by differential induration of the ash flows, resulting in units of varying hardness. The base of the Tshirege rests on the irregular erosional surface of the Otowi.

Physical properties of the tuff that may affect fluid flow result primarily from induration (which includes vapor-phase crystallization, devitrification, and welding) and jointing.

Vapor-phase crystallization results from the ash flows being partially fluidized by hot expanding gases during emplacement. After stabilization of the flows, these gases migrated upward and deposited dissolved materials as secondary minerals in void spaces between the glass shards. Vapor-phase minerals are predominantly cristobalite, alkalic feldspar, and tridymite. If a flow becomes welded before the vapor phase escapes, trapped gases may form cavities, which may or may not subsequently be filled with a solid phase.

Because volcanic glass (the major constituent of ash) is geologically unstable, it will spontaneously devitrify, yielding cristobalite, feldspar, and tridymite. Devitrification tends to be more prevalent in tuff that has undergone compaction and welding but may occur in more porous tuffs as well. Vapor-phase crystallization and devitrification can affect the hardness and porosity of the rock.

Depending on the temperature and water content of an ash flow, the constituent glass shards may deform and stick to one another, a process known as welding. Welding results in increased hardness and decreased porosity of the rock. The degree of welding in the Bandelier Tuff varies markedly. The majority of the Tshirege Member is moderately welded with some areas of more dense welding in the uppermost flow units (DOE/EIS-0018, 1979). Table I shows the variation in physical properties of the tuff as a result of welding.

Joints, formed by cooling of the ash flows, commonly divide the tuff into irregular blocks. The predominant joint sets are vertical or nearly vertical and joint frequency generally increases with increasing degree of welding. Joints range from closed to open as much as several centimeters; they may contain caliche near the surface, grading downward to clay (usually montmorillonite). In excavations, plant roots have been observed to extend to depths of at least 10 m in joints.

Moisture infiltrating into exposed tuff surfaces dissolves minute amounts of silica, which are redeposited as interstitial opaline material upon evaporation. This results in a "case hardened" surface layer a few centimeters thick that is highly resistant to wind and water erosion (DOE/EIS-0018, 1979). However, exposed pumice fragments weather readily, leaving a pitted surface on some units.

**TABLE I**  
**PROPERTIES OF TUFF AS A FUNCTION OF DEGREE OF WELDING<sup>a</sup>**

	Nonwelded	Moderately Welded	Welded
Porosity (Vol %)	40-60	30-55	15-40
Cohesion of Shards	slight	moderate	good
Deformation of Shards	none	slight	strong, flattening of shards
Fracture	crumbly	somewhat brittle	brittle

<sup>a</sup>Data from DOE/EIS-0018,1979

## B. Tuff Structure and Texture

The porosity of the tuff can be calculated from the real and apparent specific gravity where the per cent pore space =

$$1 - \frac{\text{bulk specific gravity}}{\text{real specific gravity}} \times 100 .$$

The porosity of the tuff ranges from about 20% to about 60%. The size distribution of the pores, though, may be more important than total porosity in assessing aeration, permeability, and water-holding properties.

Equivalent pore size and matric potential applied to tuff relate in the following manner.

Pore Diameter (m)	Matric Potential (kPa)
$2 \cdot 10^{-4}$	1.5
$1 \cdot 10^{-4}$	3.0
$5 \cdot 10^{-5}$	6.0
$2 \cdot 10^{-5}$	15.0

The Tshirege Member reaches porosities of 60% that are comparable to those of the upper ranges encountered in fine clays (Abrahams, 1963). Such high porosities are, however, unusual for consolidated materials.

Abrahams shows that the bulk specific gravity of dry tuff can be divided into four separate, statistically significant groups, ranging from 1280 to 1840  $\text{kg m}^{-3}$ .

There is, of course, a strong inverse correlation between the dry unit weight and porosity, while permeability has been shown to increase exponentially with the particle size and subsequent pore size. Particle sizes in the tuff average 46% of clay and silt and 53% sand and resembles a sandy silt (Abrahams, 1963).

Water in the smaller pores moves mostly by the slower processes of capillarity and vapor diffusion and, at saturation, contributes little to the bulk of the movement. Jointing, though, is common throughout the Tshirege Member and is sediment-free below a certain depth. Interconnected joints could provide paths for rapid water movement at saturation, if such a situation were to occur. Fears for this to happen are, however, unwarranted.

## C. General Climatology

Maximum temperatures are generally below 32°C, with the extreme recorded at 35°C. A large diurnal variation keeps nocturnal temperatures in the 12°C to 15°C range. Winter temperatures are typically in the range of -10°C to 5°C, with the extreme recorded at -28°C. Many winter days are clear with light winds, and strong solar radiation makes conditions quite comfortable even when air temperatures are cold. The annual total of heating °C days is 3500, with January accounting for over 610 while July and August average zero degree days. Higher temperatures will increase evapotranspiration and occur at the origin of tuff desiccation. An annual observed value of about two-thirds the potential insolation is observed based on measured diurnal direct radiation. The reduction is caused by cloudiness, implying that approximately one-third of the daylight hours in one year were affected by cloudiness. The maximum cloud-free month (January) had 85% of potential insolation while the minimum (July) had 55%. A higher insolation with the same air temperature means a higher degree of desiccation of the tuff because of increased ground temperatures from radiation absorption.

Average relative humidity is 40%, ranging from 30% in May and June to above 50% in July, January, and February. The diurnal variation is very large and basically inverted to the diurnal temperature cycle. The summer months have nocturnal maxima of 80% and minima of 30%, while spring, the driest time, has a diurnal range from 15% to 50%. A lower relative humidity will enhance desiccation of the tuff because of an increased vapor pressure differential at the ground-atmosphere interface. A high relative humidity, however, may cause condensation to occur at the tuff surface provided the temperature depression in the tuff is sufficient.

At most sites near-calm wind conditions exist 10% to 15% of the time; 80% of the wind speeds are less than  $3 \text{ m s}^{-1}$ , and less than 1% of the time 10-minute-averaged winds are greater than  $16 \text{ m s}^{-1}$ . The nocturnal period, from 2000 to 0800 MST, is representative of stable thermal stratification. The nighttime winds show the greatest incidence of calm conditions.

During the period of insolation, 0800 to 1600 MST, the air is generally unstable, and 1600 to 2000 MST is a transition period during which the statistics are strongly affected by transient processes associated with sunset. Winds will remove layers of increased vapor pressure at the ground-atmosphere interface and consequently enhance desiccation of the tuff with increased wind speed.

Atmospheric diffusion depends on three primary considerations; source factors (size, duration, elevation above ground, temperature), terrain factors (roughness, slope, vegetative cover, solar heating), and meteorological factors (wind speed and direction, temperature stratification, turbulence energy). There is considerable interdependency among all of the factors listed and many of the available formulae for estimating atmospheric dispersion represent attempts at interrelating the impact of these factors. All these factors have to be taken into consideration in evaluating the tritiated water contamination of the atmosphere.

As expected, there is a distinct orientation of the concentration pattern parallel to the canyons. This feature suggests an important role of drainage winds in transporting effluents released in the western portion of the laboratory site. Stable thermal stratification is an integral feature of the drainage winds, as is a reduced level of turbulence. Therefore, these flows, quite frequent during nighttime hours, have the poorest capacity for dilution of released material. The stable temperature stratification inhibits vertical mixing, and horizontal mixing is constrained by the presence of the canyon walls. For purposes of estimation, the dilution within short travel distances may be neglected. Hence, for drainage within canyons that open into populated areas, the effective mixing length from release point to receptor is severely reduced. In particular, sites that have a drainage wind component into Pajarito Canyon can produce abnormally high concentrations of effluents in White Rock.

Another complicated transport process relevant to potential dispersion of materials from sites located in the bottom of canyons has been identified. Two mechanisms have been documented that can lead to an exchange of air between canyon and mesa tops. The first is convective mixing in an unstable atmosphere. This is basically a daytime phenomenon, probably most prevalent in the warm season. The second mechanism occurs under all stabilities when the cross-canyon wind exceeds  $2 \text{ m s}^{-1}$ , giving rise to a major roll eddy. This means that there are many circumstances under which material could be readily transported from the canyon bottom to the mesa top. (DOE/EIS-0018, 1979, pp. 3-28 to 3-33).

#### D. Precipitation

1. **Recent Climatic Records.** The most important climatic element influencing the geohydrology of any given area is precipitation. Based on updated climatic records (1951 to 1980) for Los Alamos, New Mexico, precipitation equal to or less than an expected amount has been calculated for probability levels of 0.01 to 0.99. These values were determined based on the normal distribution obtained from precipitation data recorded in the last 30 years. Table II indicates those values on a yearly basis and shows that there is a 0.99 chance that the annual precipitation is less than 768 mm. It can also be interpreted that there is a 0.01 chance that the annual precipitation will exceed 768 mm. The updated (1980) mean annual precipitation for Los Alamos is 457 mm.

**TABLE II**  
**UPDATED PRECIPITATION WITH PROBABILITY LEVELS**  
**EQUAL TO OR LESS THAN (mm of ppt)**

Level	0.01	0.05	0.10	0.20	0.30	0.40	0.50	0.60	0.70	0.80	0.90	0.95	0.99
Ppt	146	216	259	303	333	356	457	558	581	611	655	698	768

2. **Tree-Ring Evidence.** Dendroclimatology involves comparing modern meteorological records with contemporaneous tree ring widths and establishing, through regression analysis, the best statistical relationship existing between the tree ring index as the independent variable and, say, precipitation as the dependent variable. By then substituting tree ring indices in the equation, an estimate is obtained of previous precipitation patterns. Regions where temperature or rainfall is a severely limiting factor in growth yield the most clearly interpretable climatic indices. In Los Alamos, the one factor that can be notably limiting is precipitation. This should stimulate backward extension of precipitation gauge records by growth indices. The University of Arizona has supported a continuing search throughout the Western United States for the most sensitive trees, a fundamental phase of a research program with its main objective the derivation of centuries-long rainfall indices of quantitative value. No other region in the world is apparently so naturally favored as a source of dendroclimatic history (Schulman, 1951, 1952). Long-lived coniferous species, with abilities to survive very arid cycles, make selective studies possible. Tree ring indices have been obtained that showed a high dependency on annual rainfall.

In Los Alamos, the best correlations between tree ring indices and annual precipitation were found for the following, in order of goodness of fit:

- a. Ponderosa pines, where precipitation (mm) =  $543 I_{Po}^{0.606}$ . The corresponding correlation coefficient was found to be significant at the 0.99 level ( $I_{Po}$  = tree ring index for ponderosa pine).
- b. Piñon, where precipitation (mm) =  $467 I_{Pi}^{0.619}$ . The correlation coefficient in this case was found to be still significant at the 0.99 level ( $I_{Pi}$  = tree ring index for piñon).

The similarity between these two equations is striking. The fact that in both cases the exponent of the index is  $< 1$  indicates that relatively small increases in precipitation could lead to sizable increases of tree ring indices in the Los Alamos area. A 100% increase of the index (doubling) corresponds to a 50% increase in precipitation, while a 50% decrease of the index (halving) represents a 33% decrease in precipitation.

The comparison between modern meteorological records and contemporaneous tree ring indices involves only the last 30 years. The mean tree ring index of 1, on the other hand, is based on records dating back to 1510 for ponderosa pine. If we substitute the mean tree ring index of 1 in the above formulae, a precipitation is obtained that is higher than the mean precipitation recorded during the last 30 years, because of a coefficient (e.g., 543) whose value exceeds the actual mean precipitation. This higher coefficient is because, during the 30 years to which the regression analysis was applied, the tree ring index was below average or  $< 1$ . This also implies that during the period in question, precipitation was below average since 1510.

In conclusion, there seems to be agreement that an analysis of recent past recordings in the form of either climatic records or tree ring indices, is a good way to estimate the range of future pluvial variability.

The statistical relationship established between modern pluviometric records and contemporaneous tree ring indices allows one to estimate previous precipitation patterns. Good existing correlations for ponderosa pine permitted us to make the following estimates.

- a. In the last 100 years, a maximum tree ring index of 1.85 occurred in 1919. Through regression analysis and use of derived formulae, this corresponds to an annual precipitation of 788 mm. 3/02
- b. In the last 200 years a maximum tree ring index of 2.10 occurred in 1794. Through regression analysis and use of derived formulae, this corresponds to an annual precipitation of 851 mm. 33.50
- c. The maximum tree ring index recorded in the Los Alamos area was 2.80 in 1597. This corresponds to an annual precipitation of 1013 mm. 39.88
- d. The minimum tree ring indices recorded were in the years 1523, 1524, 1585, and 1685. According to the regression equation, this corresponds to annual precipitations of 144, 144, 113, and 58 mm, respectively. Statistics based on pluviometric records indicate that annual precipitation not exceeding 146 mm is likely to occur once in 100 years.

The above precipitation estimates correspond remarkably well with the estimated occurrences of maximum precipitation based on climatic records. Table I indicates that a maximum precipitation of 768 mm can be expected every century. This is only 2.5% different from the estimate reached by tree ring index analysis (Abeele, 1980).

### III. SURFACE WATER

This section is a slightly modified version of DOE/EIS-0018, pp. 3-17 to 3-25, Final Environmental Impact Statement-Los Alamos Scientific Laboratory Site; U. S. Dept. of Energy, December 1979.

The Rio Grande, the master stream of the region, drains more than 37 000 km<sup>2</sup> in northern New Mexico and Colorado. The average discharge of the Rio Grande at the Otowi Bridge gauging station was about  $1 \cdot 10^9$  m<sup>3</sup> per year or an average of 32 m<sup>3</sup>s<sup>-1</sup> for the 1955 to 1974 period. Suspended sediments discharged at the station for the period 1947 to 1974 ranged from 0.03 kg s<sup>-1</sup> to 3900 kg s<sup>-1</sup>.

Cochiti is a new reservoir, which began filling in 1976 (Fig. 3). It is designed to provide flood control, sediment retention, recreation, and fishery development. The dam is a 9-km-long, earthfilled dam located on the Rio Grande about 30 km southwest of Otowi Bridge and about 15 km from the southernmost point of the Laboratory boundary. The  $5 \cdot 10^6$  m<sup>2</sup> surface area permanent pool will extend upstream approximately 12 km, reaching a point about 5 km from the southernmost point of the Laboratory boundary and will have a capacity of nearly  $62 \cdot 10^6$  m<sup>3</sup>. The flood-control pool extends upstream to the Otowi Bridge with a total volume of  $750 \cdot 10^6$  m<sup>3</sup>.

Essentially all downstream flow passes through the reservoir. Flood flows are temporarily stored and released at safe rates. The sediment-trapping function of the dam is expected to trap at least 90% of the sediments carried by the Rio Grande. Approximately  $6.2 \cdot 10^6$  m<sup>3</sup> per year will be lost to evaporation from the permanent pool.

There are no municipal water supplies taken directly from the Rio Grande downstream from Los Alamos National Laboratory in New Mexico. Irrigation water is taken from the Rio Grande downstream from the Laboratory at numerous diversions starting below Cochiti Dam.

The quality of surface waters in the Upper Rio Grande Basin is generally good. The bacterial and chemical quality of all streams, with the exception of a reach of the Rio Grande between Española and Otowi Bridge, is considerably better than that required by the New Mexico State Water Quality Control Commission stream standards. The poor quality below Española to Otowi Bridge is attributed to the population concentration in the Española Valley. This reach is upstream of Los Alamos.

In the Los Alamos area, there is intermittent stream flow in canyons cut into the Pajarito Plateau. Perennial flow to the Rio Grande occurs in the Rito de los Frijoles to the south of the Laboratory and Santa Clara Canyon to the north. Springs between 2400- and 2700-m elevation on the slopes of the Sierra de los Valles supply base flow throughout the year to the upper reaches of Guaje, Los Alamos, Pajarito,

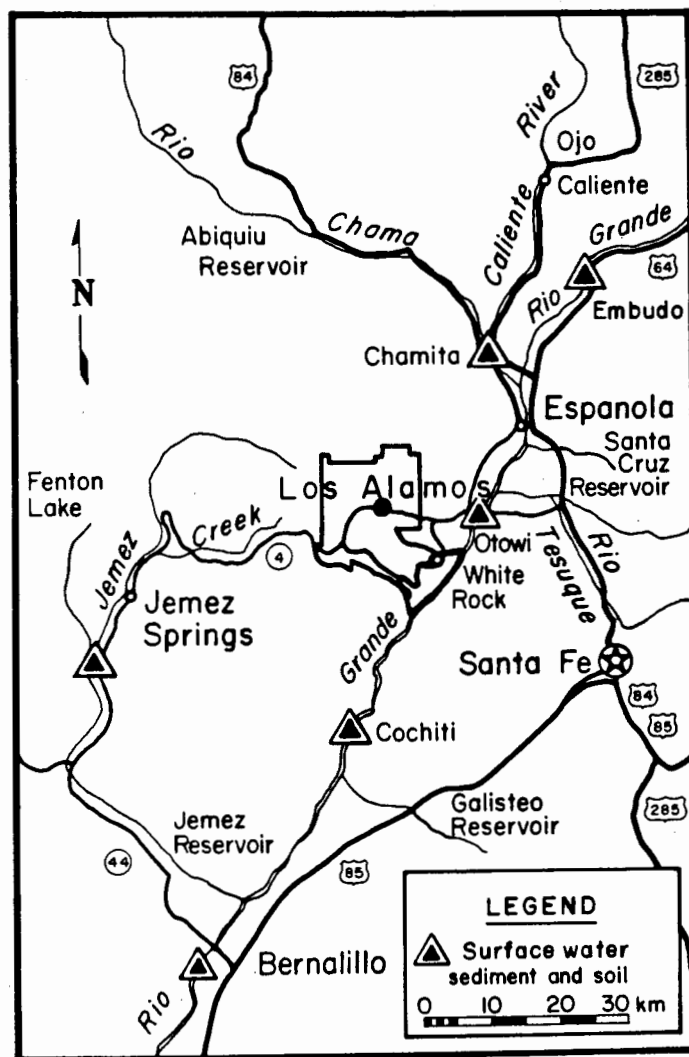


Fig. 3. Base map.

and Water Canyons, and Canyon del Valle. These springs discharge water perched in the Bandelier Tuff and Tschicoma Formation at rates from  $1 \cdot 10^{-4}$  to  $9 \cdot 10^{-3} \text{ m}^3 \text{ s}^{-1}$ . The volume of flow from the springs is insufficient to maintain surface flow within more than the western third of the canyons before it is depleted by evaporation, transpiration, and infiltration into the underlying alluvium.

Sixteen drainage areas, with a total area of  $212 \text{ km}^2$ , pass through or originate within the Laboratory boundaries. Stream flow in these canyons is intermittent. Runoff from heavy thunderstorms or unusually heavy snowmelt will reach the Rio Grande. Four canyons — Pueblo, Los Alamos, Pajarito, and Water — have areas greater than  $20 \text{ km}^2$ . Ancho Canyon has  $17 \text{ km}^2$ , and all the rest have less than  $10 \text{ km}^2$ . Theoretical flood frequency and maximum discharge in 10 of the well-defined channels of the 16 drainage areas range from  $1.1 \text{ m}^3 \text{ s}^{-1}$  for a two-year frequency to  $21 \text{ m}^3 \text{ s}^{-1}$  for a 50-year frequency. Flooding does not pose a problem in the Los Alamos area. Highways may occasionally be closed for an hour when flash floods in canyons cross the pavement. Nearly all community and Laboratory structures are located on the mesa tops, which drain rapidly into the deep canyons.

Pajarito Site is located in Pajarito Canyon below a drainage area of  $26 \text{ km}^2$ . The 100-year storm (i.e., probability 0.01 in any year) will result in a discharge of  $31 \text{ m}^3 \text{ s}^{-1}$ . The channel at the site that is restricted by a bridge will carry  $42 \text{ m}^3 \text{ s}^{-1}$ .

Omega Site and W-Site are located in Los Alamos Canyon near the western edge of the Pajarito Plateau. The two sites are about 600 m apart with a drainage area of about 20.5 km<sup>2</sup> above the sites. The 100-year storm would produce a maximum flow of about 25 m<sup>3</sup> s<sup>-1</sup> at the sites. An extrapolation indicates a 500-year flood (i.e., probability 0.002 in any year) would have a peak flow of about 37 m<sup>3</sup> s<sup>-1</sup>.

A box culvert at W-Site extends under the parking lot and has a carrying capacity of 156 m<sup>3</sup> s<sup>-1</sup>, while a restriction at the entrance of the channel at Omega Site will carry about 46 m<sup>3</sup> s<sup>-1</sup>. Thus, the channels at both sites should carry the maximum flow of 25 m<sup>3</sup> s<sup>-1</sup> produced by a 100-year storm. If the channel should become clogged with debris, the resulting overflow would be carried by roadways or parking lots adjacent to the channel and would not cause damage to the structures in the area.

Another flood hazard considered was failure of the Los Alamos Canyon Reservoir. The dam is a concrete-core, rock and earthfilled dam with a capacity of 4.9 · 10<sup>4</sup> m<sup>3</sup>. The concrete spillway will carry a flow of 16 m<sup>3</sup> s<sup>-1</sup>, which is ample for the estimated flow of 12 m<sup>3</sup> s<sup>-1</sup> produced by a 100-year storm.

Sanitary sewage effluents from both the townsite and the Laboratory are released into Pueblo and Sandia Canyons in sufficient volume to saturate the alluvium and maintain surface flows for a few hundred meters. Mortandad Canyon contains a small perennial stream maintained for about 1.5 km by effluents from a Laboratory cooling tower and an industrial-waste treatment plant.

#### IV. SATURATED FLOW

Ground water (subsurface water) occurs as perched water in alluvium and basalts and, in the zone of saturation, in sediments of the main aquifer of the Los Alamos area.

Two types of alluvium have developed in the stream channel. Drainage areas heading on the mountain flanks are made up of sand, gravels, cobbles, and boulders derived from the Tschicoma Formation and Bandelier Tuff. Drainage heading on the plateau contains only sands, gravels, and cobbles derived from the Bandelier Tuff. The alluvium is quite permeable, allowing rapid infiltration of rainfall and streamflow. The alluvium generally overlies the less permeable tuff. Water infiltrates downward in the alluvium until its movement is held back by the tuff. This results in the build-up of ground water perched within the alluvium. Saturated hydraulic conductivity of the alluvium ranges from 1.65 · 10<sup>-3</sup> m s<sup>-1</sup> for a sand aquifer to 5.8 · 10<sup>-4</sup> m s<sup>-1</sup> for a silty sand aquifer.

As water perched in the alluvium moves down the gradient, it is lost by evaporation and transpiration through plants and infiltration into underlying tuff. Vegetation is lush where surface or perched water in the alluvium is present. Water moving from the alluvium into the volcanic debris in the lower reach of Pueblo Canyon and the midreach of Los Alamos Canyon recharges a local body of perched water within the basaltic rock of Chino Mesa. Water from this perched aquifer discharges at the base of the basalt in Los Alamos Canyon west of the Rio Grande.

The hydraulic conductivity of this perched aquifer is 1.32 · 10<sup>-3</sup> m s<sup>-1</sup>.

Perched water is not found in the tuff, volcanic sediments, or basalts above the main aquifer in the central and western portions of the Plateau. Test holes in these areas penetrated numerous rock units that had the potential of perching water above the main aquifer. The absence of water in these test holes indicates that the infiltration of surface water through the alluvium and the tuff is limited. Age dating of water from the main aquifer further supports the inference of insignificant infiltration of surface water through the alluvium and tuff to the main aquifer.

The main aquifer in the Los Alamos area is located within the Tesuque Formation beneath the entire Plateau and Rio Grande Valley. The lower part of the Puye Conglomerate as well as the Tesuque Formation are within the main aquifer beneath the central and western portions of the Plateau. The depths to water below the mesa tops range from about 360 m along the western margin of the Plateau to about 180 m along the eastern part of the Plateau. The thickness of potable water in the aquifer is estimated to be at least 1200 m. The hydraulic gradient of the aquifer averages about 1.1% within the Puye Conglomerate but increases to about 20% along the eastern edge of the Plateau as the water in the aquifer enters the less permeable sediments of the Tesuque Formation. The average movement rate within the aquifer is about 3.5 · 10<sup>-6</sup> m s<sup>-1</sup> toward the Rio Grande.

The hydraulic conductivity and transmissivity are different for various rock units within the main aquifer. Aquifer tests in wells penetrating the Puye Conglomerate indicated saturated hydraulic conductivities ranging from less than  $1.15 \cdot 10^{-5} \text{ m s}^{-1}$  to  $1.50 \cdot 10^{-4} \text{ m s}^{-1}$ . Supply wells in the Los Alamos Field penetrating sediments of the Tesuque Formation have an average transmissivity of  $2.3 \cdot 10^{-3} \text{ m}^2 \text{ s}^{-1}$ , with an average hydraulic conductivity of less than  $10^{-5} \text{ m s}^{-1}$ . The wells in the Guaje Field, which penetrate basalts interbedded with sediments in the Tesuque Formation, have an average transmissivity of about  $2.5 \text{ m}^2 \text{ s}^{-1}$ , with an average hydraulic conductivity of about  $10^{-5} \text{ m s}^{-1}$ . Supply wells in the Pajarito Well Field penetrated basalts interbedded with sediments in the Puye Conglomerate and the Tesuque Formation. The transmissivities ranged from  $6 \cdot 10^{-3}$  to  $4.6 \cdot 10^{-2} \text{ m}^2 \text{ s}^{-1}$ . The aquifer is under water table conditions in the western portion of the Plateau. Along the eastern margins the aquifer is artesian; that is, the water level in a well penetrating the aquifer will rise above the top of the saturated water-bearing material.

The major recharge area for the deep aquifer is in the intermountain basins formed by the Valles Caldera. The saturated sediments and volcanics in the basins are highly permeable and recharge the main aquifer in sediments of the Tesuque Formation and Puye Conglomerate. Minor amounts of recharge may occur in the deep canyons containing perennial streams on the flanks of the mountains.

The movement of water in the main aquifer is eastward toward the Rio Grande, where a part is discharged through springs and seeps into the river. It is estimated that the 18.4 km reach through White Rock Canyon below Otowi Bridge receives a discharge from the aquifer of  $5.3$  to  $6.8 \cdot 10^6 \text{ m}^3$  annually or an average of  $1.92 \cdot 10^{-1} \text{ m}^3 \text{ s}^{-1}$ .

## V. GAUGING STATION, AREA G

### A. Introduction

A potential exists for transport of radionuclides out of disposal sites by surface runoff. A gauging station was constructed at Area G, TA-54, to provide a sediment sampling point and to determine the volume of runoff from a representative portion of the area. Rainfall-runoff data from the gauging station will also be used to validate simulation models of the water balance at the disposal sites.

A catchment basin was constructed near the outlet of a major drainage from the site. A dam at the downstream end of the basin was fitted with a weir plate for discharge measurements.

### B. Location and Watershed Area

The location of the weir is indicated in Fig. 4, as is the outline of the area draining through the weir. Asphalt runoff channels are indicated. There is a cutoff ditch along the slope north of the drainage basin, which directs flow to a discharge point below the weir. The total effective drainage area is  $34\,500 \text{ m}^2$ , with slopes varying between 5 and 25%. The average slope for the watershed is about 10%.

### C. Weir and Stilling Basin

A cross section of the weir dam is shown in Fig. 5. An aluminum weir plate, with a beveled  $90^\circ$  notch, was installed in the dam (Fig. 6). A cleaning port, sealed with a removable cover, is located in the bottom third of the plate.

The cross section (Fig. 5) also shows the original stilling basin profile. Sediment accumulation alters the volume of the basin below the weir notch with each runoff event. The volume of the basin from an elevation level with the bottom of the cleaning port to the bottom of the notch is approximately  $17 \text{ m}^3$ .

The water level in the stilling basin is recorded by a water level gauge installed in a stilling well (Fig. 5). The recorder is equipped with a spring-driven clock, adjustable for 1-day or 7-day service time. A special trigger mechanism starts the clock when the recorder float starts upward. Thus, the discharge record begins essentially at the start of each runoff event.

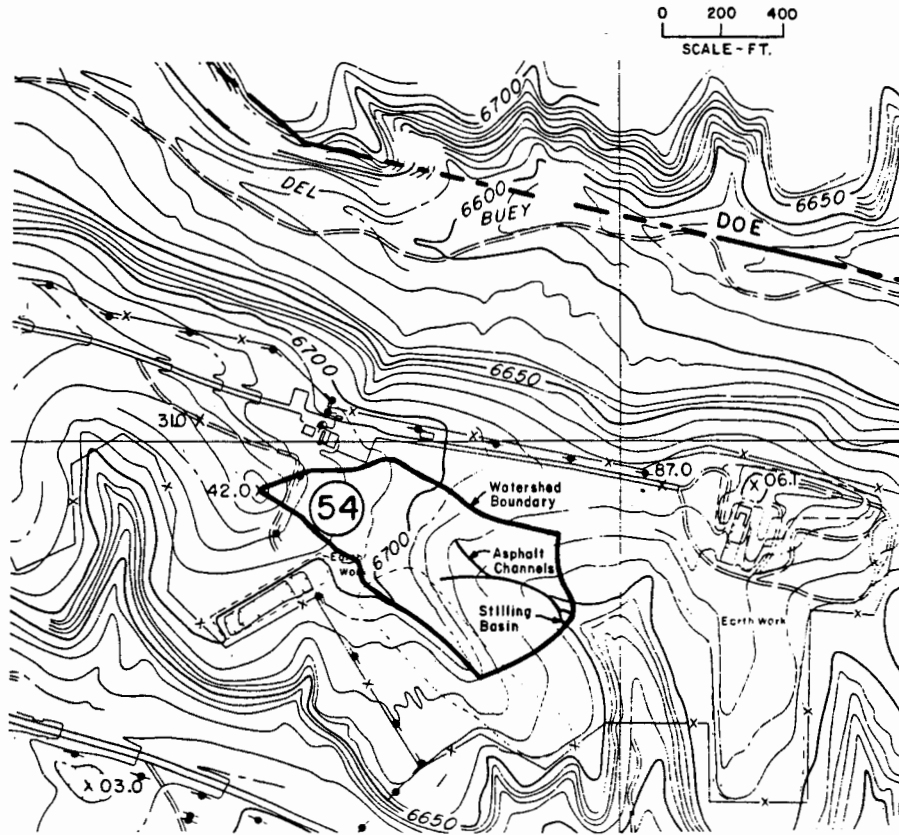


Fig. 4. Location of watershed and stilling basin, Area G, TA-54.

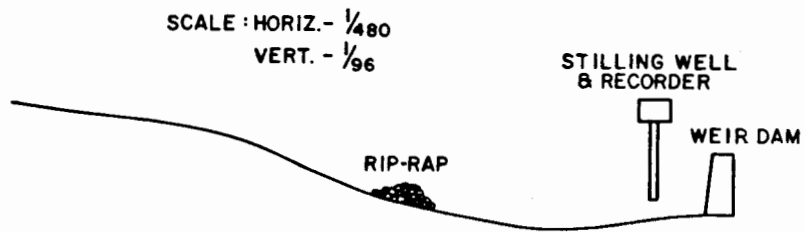


Fig. 5. Cross section of stilling basin.

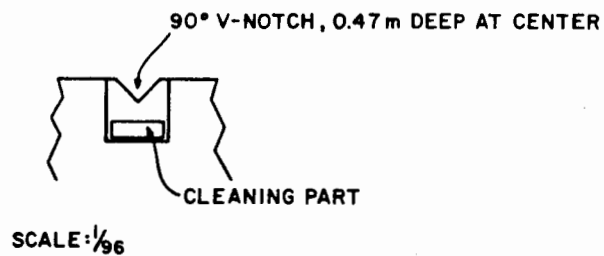


Fig. 6. Weir plate details.

## D. Runoff Events

Installation of the recorder and weir was completed by mid-summer 1980. A major storm on 18 August produced runoff, but the recorder malfunctioned, and no runoff data were obtained; however, cumulative samplers downgradient from the weir were used to collect runoff samples (solution and suspended sediments) for plutonium analyses. The analyses were performed to determine if there was any measurable transport of plutonium from the surface of Area G. A similar sample was collected outside area G to provide background for the runoff event. The background analyses and analyses from the cumulative samplers were below the mean limits of detection for plutonium (<5 pCi/l solution; 1 pCi/g suspended sediments).

A second storm complex delivered a total of 22.1 mm between 8 and 10 September 1980.

The hydrograph for 9 September 1980, together with observed precipitation, is given in Fig. 7. From 0100 hours on 10 September 1980, the water level showed a continuing decline caused by evaporation and gradual leakage from the stilling pond.

## E. Weir Calibration

1. Theoretical. The discharge through a 90° V-notch weir is expressed by

$$Q = \frac{8}{15} \sqrt{2g} C_d h^{5/2} = 2.36 C_d h^{5/2}, \quad (1)$$

where

Q = Discharge -  $m^3 s^{-1}$ ,  
g = Acceleration of gravity,  
 $C_d$  = Coefficient of discharge, and  
h = Water height above V-notch.

The value of  $C_d$  is approximately 1.0 but varies as an empirical function of the weir.

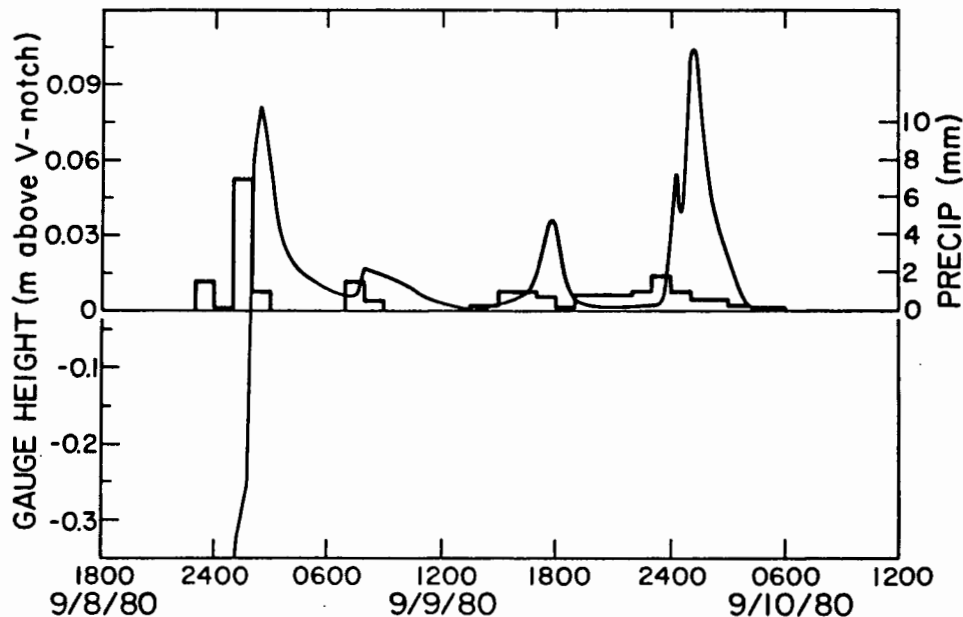


Fig. 7. Precipitation and runoff, Area G weir.

2. Empirical. A period was selected on 9 September 1980, when flow was occurring through the weir. A sequence of measurements was made, recording the time required for a fixed volume to flow through the weir. The water height, "h," was also recorded.

The measured discharge data are given in Table III.

The value of  $C_d$  for this weir can be determined, using Eq. (1), and the measured values of Q and h.

$$C_d = \frac{Q}{2.36 h^{5/2}} = \frac{3.3 \cdot 10^5 \text{ m}^3 \text{ s}^{-1}}{2.36 (1.21 \cdot 10^{-2})^{5/2}} = 0.87 .$$

Thus, for flow in this range of discharge, the weir calibration is

$$Q = 2.1 h^{5/2} .$$

Further calibration will be required to extend this relationship to significantly higher discharges.

#### F. Rainfall-Runoff Calibration

The storm event can also be used to evaluate the relationship between precipitation and runoff from the watershed. A rational formula is commonly used to estimate the peak discharge from precipitation on a small watershed. For conditions on this watershed the equation is

$$Q = 1.1 \cdot 10^{-7} (i) (A) ,$$

where

- Q = Peak discharge,  $\text{m}^3 \text{ s}^{-1}$
- i = Precipitation rate, mm/h, and
- A = Drainage area,  $\text{m}^2$ .

The observed precipitation and runoff are tabulated in Table IV, together with discharge calculated by the above formula.

The comparison shows that estimated discharges are significantly larger than measured values. However, the runoff formula is most applicable to high intensity storms (>25 mm/h) of 30 min to 1 h

TABLE III  
DISCHARGE DATA FOR AREA G WEIR

Measurement Number	Flow (ℓ)	Elapsed Time (sec)	Discharge Rate ( $\text{m}^3 \text{ s}^{-1}$ )	Water Height (m)
1	3.5	105	$3.3 \cdot 10^{-5}$	$1.21 \cdot 10^{-2}$
2	3.5	113	$3.3 \cdot 10^{-5}$	$1.21 \cdot 10^{-2}$
3	3.5	113	$3.1 \cdot 10^{-5}$	$1.21 \cdot 10^{-2}$
		mean	$3.3 \cdot 10^{-5}$	$1.2 \cdot 10^{-2}$

**TABLE IV**  
**PRECIPITATION AND RUNOFF ON JULY 10, 1980**

Time (hr)	Precipitation (mm/hr)	Discharge- $\text{m}^3 \text{ s}^{-1}$	
		Observed	Calculated
1500	0.3	$6 \cdot 10^{-6}$	$1.2 \cdot 10^{-3}$
1600	1.0	$6 \cdot 10^{-6}$	$3.8 \cdot 10^{-3}$
1700	1.0	$9 \cdot 10^{-5}$	$3.8 \cdot 10^{-3}$
1800	0.8	$3.2 \cdot 10^{-4}$	$3.0 \cdot 10^{-3}$
1900	0.3	$1.3 \cdot 10^{-4}$	$1.2 \cdot 10^{-3}$

duration. Overestimation of discharge for small storms results from excessive infiltration and evaporation compared with larger storms. Further work, involving the inclusion of the dynamics of the rainfall-runoff process, may be required to improve agreement between estimated and actual runoffs. At present, the weir and stilling basin appear to be adequately sized for expected discharges.

## VI. SATURATED AND UNSATURATED HYDRAULIC CONDUCTIVITIES

### A. General

Precipitation, if occurring persistently and in large amounts, may reach the waste material in a disposal pit. Because potential evapotranspiration exceeds precipitation at the disposal sites, the majority of the percolating water is evaporated long before it reaches the waste material. The bottom of the soil horizon, consisting of a pronounced clay, is generally less than a meter deep. The clay horizon effectively restricts any further downward movement of water into the underlying Bandelier Tuff, where all the waste disposal sites at Los Alamos are located.

The fractures and joints are commonly filled with fine-grained weathering products within 10 m from the surface, while being open at greater depth with no sign of weathering. Roots penetrate filled fractures, attracted by the higher moisture availability in finer materials. Montmorillonite, present in considerable amount among the finer materials and expanding upon wetting, will seal fractures and strongly inhibit moisture movement. Moisture monitoring by means of a neutron moisture probe indicates that at depths exceeding 10 m the tuff rarely exceeds 10% of saturation. At such a low moisture ratio, only unsaturated and vapor flow can occur. As the degree of unsaturation augments, movement in the vapor phase becomes more preponderant. Here one needs to remember that fractures or joints, which are effective barriers to liquid unsaturated flow, are open pathways for unhindered diffusion of water in the vapor phase. Tritiated water vapor migration is consequently enhanced by the presence of such transportation channels. It must be remembered, however, that tritium is the only radionuclide at Los Alamos disposal sites to travel in the gaseous phase. All other radionuclides can be removed from their original location only through the movement of liquid water, barring a catastrophic event. Because fractures will act as barriers for unsaturated liquid flow, all radionuclides, except tritium, will be inhibited by the presence of these fractures in their movements through the tuff. Existence of low moisture content is further proven historically by the absence of weathering below 10 m (Wheeler et al., 1977). The hydraulic conductivity decreases strongly with the degree of saturation. The hydraulic conductivity was found to be a power function of the saturation ratio and will be expressed as such in the following chapters.

Saturation ratios of crushed fill overlying waste disposal pits remain constant below 3 m at a saturation ratio of 0.1 without even a sign of a significant seasonal variation.

Forces causing significant moisture movement result from gravity, moisture gradients, and temperature gradients. A difference in temperature or moisture content will also be the motive force to diffusion in the vapor phase. A moist or warm soil in contact with a dry or cool soil will create a vapor pressure gradient and a vapor diffusion into the drier or cooler area will occur.

Vertical liquid water flow at depths greater than 10 m, where there is no vapor pressure gradient, will be mainly a function of the hydraulic gradient ( $\frac{h}{L}$ ), which is the energy loss per unit weight or head loss divided by the length of flow. Further, the vertical liquid water flow will be a function of the hydraulic conductivity of the tuff at a particular water content ( $K_\theta$ ). The moisture flow per unit area will consequently be described as

$$q = K_\theta \frac{h}{L} .$$

## B. Crushed Tuff

1. Measurements. The essential parts of the laboratory apparatus used included a volumetric pressure plate extractor with a cell pressure control system accurate to 0.25%. The porous plate had a bubbling pressure of 200 kPa. The outflow measurement system consisted of a sealed Erlenmeyer flask into which the water was released. The flask was placed on a Mettler balance, which allowed for continuous weighing of the outflow. A burette was used to remove air from beneath the porous plate.

The simplest technique, described by Klute (1965), was first used to determine the unsaturated hydraulic conductivity. Although the experimental technique itself seemed to be flawless, no matching of Klute's theoretical diffusion equation plotted as the overlay or theoretical curve and the experimentally determined volume-outflow curve could be obtained without translation of the plots. An overlay was drawn for each applied matric potential. The conclusion was consequently reached that the assumption of a negligible head loss through the porous plate was not valid.

A series of corrective outflow overlays were drawn in accordance with the method suggested by Miller and Elrick (1958) for the determination of hydraulic conductivity extended to cases with non-negligible plate impedance. The corrective translation needed to obtain the matching of any of the overlays and the experimental curves turned out to be near an order of magnitude larger than Miller and Elrick assumed! Rijtema (1959) pointed out that unless good contact is established between the plate and the soil, an unknown flow impedance may prevail that could far outweigh the plate impedance itself. The plate impedance permitted a flow rate of  $3.8 \cdot 10^{-8} \text{ m}^3 \text{ s}^{-1} \text{ m}^{-2} \text{ kPa}^{-1}$  or  $1.37 \text{ cm}^3 \text{ h}^{-1} \text{ cm}^{-2} \text{ bar}^{-1}$  at saturation. The possible contact impedance could appear and grow as the matric potential or the saturation ratio was decreasing. Using Rijtema's method, the total impedance of the tuff sample is determined from the experimental outflow data for each applied matric potential (or pressure step). Data for  $1 - Q_t/Q_\infty$  are computed from the experimental values of the outflow  $Q_t$  at time  $t$  and the equilibrium yield  $Q_\infty$  obtained for a particular pressure step. Values of  $1 - Q_t/Q_\infty$  are plotted on a logarithmic scale against  $tL^{-2}$ , where  $t$  is the time elapsed for a particular outflow quantity  $Q_t$  and  $L$  is the thickness of the sample. Rijtema devised a method to calculate the diffusivity based on the ratio of the slope of the straight line drawn through the experimental points and a value derived directly from the intercept of that straight line and the  $1 - Q_t/Q_\infty$  axis. The hydraulic conductivity  $K$  at that particular pressure step can now be calculated by finding the product of the diffusivity  $D$  and the specific water capacity  $c$ . The equation for the time required for 0.99 of the outflow to occur is  $t_{0.99} = 1.68 L^2 D^{-1}$ .

This equation was used to check what the magnitude of  $D$  must be if a 1-day equilibrium time was chosen. Computations show that  $D$  should be  $2.5 \times 10^{-8} \text{ m}^2 \text{ s}^{-1}$ . It was known from past experiments that the diffusivity of Bandelier tuff normally exceeded that value at matric potentials higher than  $-200 \text{ kPa}$ . Consequently, the time for equilibrium was set at 1 day. Upon completion of the experiment, the sample was oven-dried, yielding an additional 41 g of water. The total amount of water present at

saturation was calculated to be 185 g. Knowing the dry weight of the tuff, it can be deduced that saturation is equivalent to 31% of water by weight. Table V shows how matric potential outflow, water ratio by mass, degree of saturation, specific water capacity, water diffusivity, and hydraulic conductivity correspond (Abeele, November 1979).

To determine if a thickness effect (of the soil layer under analysis) was taking place, 970 g of dry soil, 59 mm high, were put in the extractor and saturated. The total amount of water released, under a pressure of 30 kPa and 100 kPa, respectively, was measured. The ratio of released water (30 kPa vs 100 kPa) was 0.78, which is not very different from the ratio released during the former experiment (0.81). Desiccation of the soil submitted during 48 hours to a pressure of 100 kPa indicated a remaining moisture ratio of 0.789 in the top layer vs a remaining moisture ratio of 0.0893 in the bottom layer. The bulk of the soil yielded a remaining moisture ratio of 0.0847, which is very close to the one measured in the previous experiment (0.0848). This duplication seems to validate the previous experiment.

If matric potential vs saturation ratio, hydraulic conductivity vs saturation ratio, and hydraulic conductivity vs matric potential are plotted on a log-log graph, a straight line is obtained in every case corresponding to matric potentials lower than -11 kPa.

The range of matric potentials was limited to those below -11 kPa for the purpose of curve fitting because of the difficulty in measuring water outflow at the higher matric potential.

TABLE V

HYDRAULIC CHARACTERISTICS OF CRUSHED BANDELIER TUFF  
AS A FUNCTION OF MATRIC POTENTIAL  
(Specific H<sub>2</sub>O Capacity, H<sub>2</sub>O Diffusivity and Hydraulic Conductivity  
were only measured at pressure steps <10%)

Matric Potential (-kPa)	Outflow (g)	Saturation Ratio	Specific Water Capacity (m <sup>-1</sup> )	Water Diffusivity (m <sup>2</sup> s <sup>-1</sup> )	Hydraulic Conductivity (m s <sup>-1</sup> )
0	0.000	1.000			
10	20.082	0.890			
11	24.320	0.868	8.98 · 10 <sup>-2</sup>	1.02 · 10 <sup>-7</sup>	9.18 · 10 <sup>-9</sup>
30	108.128	0.415			
33	110.261	0.405	1.58 · 10 <sup>-2</sup>	2.15 · 10 <sup>-7</sup>	3.38 · 10 <sup>-9</sup>
42	117.407	0.368			
46	120.241	0.350	1.50 · 10 <sup>-2</sup>	1.38 · 10 <sup>-7</sup>	2.07 · 10 <sup>-9</sup>
60	126.241	0.318			
66	127.841	0.310	5.64 · 10 <sup>-3</sup>	1.33 · 10 <sup>-7</sup>	7.51 · 10 <sup>-10</sup>
80	131.589	0.290			
88	132.749	0.283	3.07 · 10 <sup>-3</sup>	1.40 · 10 <sup>-7</sup>	4.30 · 10 <sup>-10</sup>
96	134.437	0.273	2.98 · 10 <sup>-3</sup>	1.21 · 10 <sup>-7</sup>	3.60 · 10 <sup>-10</sup>
120	136.949	0.260			
132	137.949	0.255	1.76 · 10 <sup>-3</sup>	9.30 · 10 <sup>-8</sup>	1.64 · 10 <sup>-10</sup>
146	139.315	0.248	2.06 · 10 <sup>-3</sup>	4.80 · 10 <sup>-8</sup>	9.91 · 10 <sup>-11</sup>
161	140.543	0.240	1.73 · 10 <sup>-3</sup>	4.62 · 10 <sup>-8</sup>	8.01 · 10 <sup>-11</sup>
177	142.643	0.230	2.78 · 10 <sup>-3</sup>	1.88 · 10 <sup>-8</sup>	5.22 · 10 <sup>-11</sup>
195	144.057	0.223	1.66 · 10 <sup>-3</sup>	3.08 · 10 <sup>-8</sup>	5.13 · 10 <sup>-11</sup>

If  $\theta_v$  represents the water-filled porosity,  $\theta$  or  $(\theta/\theta_s)$  the saturation ratio,  $\psi$  the matric potential in kPa,  $K_s$  the saturated hydraulic conductivity ( $9.2 \cdot 10^{-7} \text{ m s}^{-1}$ ),  $K$  or  $K(\theta)$  the unsaturated hydraulic conductivity, and  $r^2$  the coefficient of determination, the following equations are obtained.

$$\begin{aligned} \theta &= 1.21 \psi^{-0.321}, & r^2 &= 0.993; \\ K &= 2.43 \cdot 10^{-5} \psi^{-2.475}, & r^2 &= 0.990; \\ K &= 5.04 \cdot 10^{-6} \theta^{7.623}, & r^2 &= 0.980. \end{aligned}$$

As can be seen from the high values obtained for the coefficient of correlation, the above equations, if plotted on a log-log graph, will very closely match a straight line.

**2. Predictive Methods.** Because the hydraulic conductivity-water content relationship  $K(\theta)$  is comparatively difficult to obtain, the possibility of predicting the hydraulic conductivity from the matric potential-water content relationship has been widely explored. Millington-Quirk (1961) and Campbell (1974), among others, developed equations for this purpose. Several authors treated a variety of predictive methods against experimental data and indicated the superiority of a "corrected" Millington-Quirk (MQ) method. A correction coefficient is introduced to match the observed vs the computed saturated conductivity. Jackson et al. (1965) and Kunze et al. (1968) modified the MQ formula by introducing a "matching factor" to improve the predictability of the equation. The MQ method uses the equation

$$K = 3.14 \cdot 10^{-2} \theta_v^{4/3} n^{-2} [h_1^{-2} + 3h_2^{-2} + \dots + (2n-1) h_n^{-2}] \cdot K_s/K_{sc} \text{ (m s}^{-1}\text{)} .$$

The water-filled porosity  $\theta_v$  in  $\text{cm}^3 \text{ cm}^{-3}$ , the pressure potential  $h$  in kPa and the total number of pore intervals  $n$  give the hydraulic conductivity units of  $\text{ms}^{-1}$ . In portions of the curve where data were scarce, curve fitting through regression analysis was applied to enhance the validity of the moisture characteristic curve. The constant is valid for laboratory experiments conducted at a temperature of 300K.  $K_s/K_{sc}$  is the matching factor (measured saturated conductivity/calculated saturated conductivity).

If the obtained conductivity data are fitted to the water-filled porosity, a power function is obtained where, for  $\theta_v$  ranging from 0.02 to saturation (0.40),

$$K = 7.96 \cdot 10^{-4} \theta_v^{7.379} \text{ with } r = 0.9994 \text{ and}$$

$$K = 9.2 \cdot 10^{-7} \theta^{7.379} \text{ with } r = 0.9994 .$$

As can be seen through comparison with the laboratory method (Rijtema's technique), the slopes are almost identical, the  $K(\theta_v)$  function being somewhat steeper when measured (Rijtema, 1979). This is counterbalanced by the fact that the coefficient used in Rijtema's equation is less than 5.5 times higher than in the MQ equation. Consequently, *at any point*, the measured hydraulic conductivity will be *less* than 5.5 times higher than the predicted one using the MQ method (Abeele, November 1979).

Campbell's method for determining unsaturated conductivity from moisture retention data is simpler but agrees less with the laboratory method when applied to the Bandelier Tuff. An empirical expression relating water potential to water content for limited ranges of water content is, below matric potentials of  $-11 \text{ kPa}$ ,

$$\psi = \psi_e (\theta/\theta_s)^{-b} ,$$

where  $\psi_e$  is the air-entry water potential and  $\theta_s$  the saturated water content. The slope  $b$  can be determined from the above relationship and the unsaturated hydraulic conductivity is subsequently determined from the equation

$$K = K_s (\theta/\theta_s)^{2b+2}.$$

Through regression analysis, using the moisture retention data,  $\psi/\psi_s = 0.0097(\theta/\theta_s)^{-3.0563}$ , fixing the value of  $b$  at 3.0563. The unsaturated hydraulic conductivity is subsequently expressed as

$$K = 9.2 \cdot 10^{-7} \theta^{8.113} \text{ (m s}^{-1}\text{)}.$$

Higher exponents in the three alternative regressions mean lower hydraulic conductivity, whereas higher coefficients mean higher values. Because the formula with the highest exponent is also the one with highest coefficient, the three methods result in hydraulic conductivities never exceeding one order of magnitude in difference. The superiority of the MQ method seems to be confirmed when matched with the measured values. Campbell's predictive method retains the advantage of being the easiest one to compute (Abeele, November 1979). For a graphic comparison of predicted conductivities vs measured conductivities, see Fig. 8.

A monitoring hole (GP1-1), drilled in fill material overlying a waste disposal pit, shows significant seasonal fluctuations in moisture content. The computed moisture flux was always found to be directed downward. This downward flux from the overburden averaged  $3.76 \cdot 10^{-9} \text{ m s}^{-1}$  or  $0.12 \text{ m yr}^{-1}$ . The downward flux from the overburden was computed to average  $2.94 \cdot 10^{-10} \text{ m s}^{-1}$  or  $0.09 \text{ m yr}^{-1}$  in 1978 and  $4.75 \cdot 10^{-10} \text{ m s}^{-1}$  or  $0.15 \text{ m yr}^{-1}$  in 1979. The higher average occurring in 1979 is probably caused by extremely high precipitations occurring at the end of 1978 and the beginning of 1979..

$$\text{The flux } Q = K(\theta) \frac{\Delta(h-z)}{\Delta z},$$

where

$z$  = depth,

$h$  = matric potential corresponding to measured moisture content, and

$K(\theta)$  = hydraulic conductivity corresponding to measured moisture content.

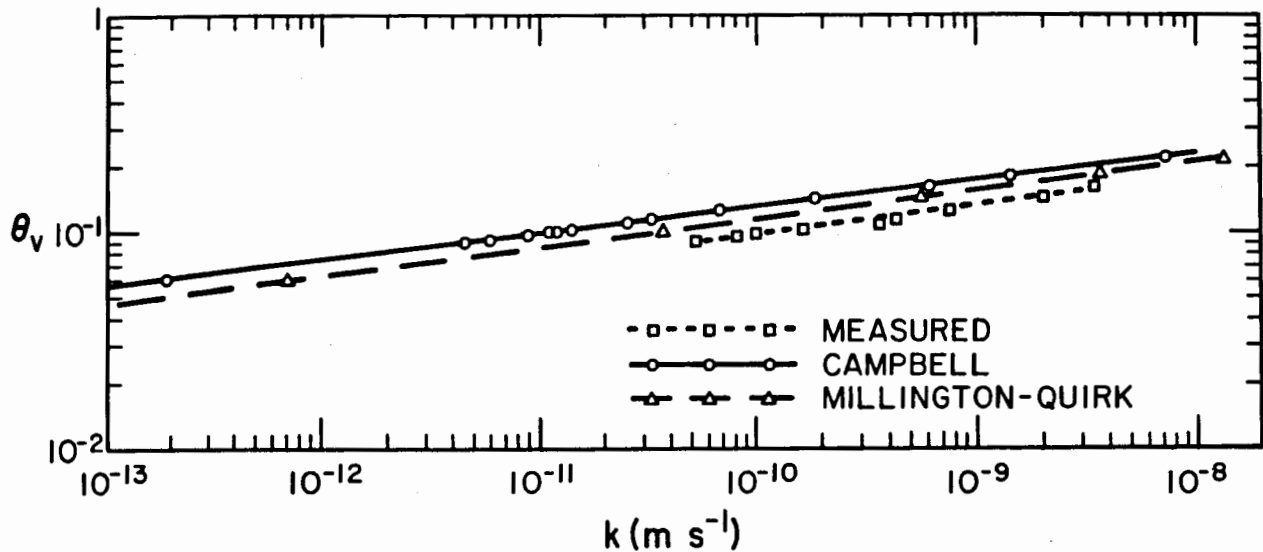


Fig. 8. Calculated hydraulic conductivities compared with measured data.

h and  $K(\theta)$  are determined from the formerly expressed regression equation. These results are higher by a factor of 3 than the flux estimated in the 1979 Annual Report where the downward moisture flux was estimated at  $9.5 \cdot 10^{-10} \text{ m s}^{-1}$ .

The maximum downward moisture flux was computed to occur in December 1978 and found to be  $2.2 \cdot 10^{-8} \text{ m s}^{-1}$  or  $0.694 \text{ m yr}^{-1}$ . This followed an extremely wet November (1978) when close to 0.17 m of precipitation fell.

### C. Solid Tuff

1. **Measurements.** The saturated hydraulic conductivity of solid tuff has been measured quite often. Widely differing measurements yield results from  $2 \cdot 10^{-7} \text{ m s}^{-1}$  to  $4.7 \cdot 10^{-6} \text{ m s}^{-1}$  when corrected for a temperature of 288K (Abrahams, 1963).

In the tuff used in these specific studies, a saturated hydraulic conductivity of  $2.35 \cdot 10^{-6} \text{ m s}^{-1}$  was measured. The unsaturated hydraulic conductivity was never measured.

2. **Predictive Methods.** The unsaturated hydraulic conductivity was predicted from the matric potential-water content relationship (moisture characteristic curve) according to the corrected MQ method. Table VI summarizes the characteristics that led to the computations of hydraulic conductivity as a function of matric potential. The acceptance of these results is based on the similarity found to exist between the predictive method according to Millington-Quirk and the measured values obtained for crushed tuff. A similar representation was assumed to exist for solid tuff.

The following equations were obtained through regression analysis for matric potentials lower than -15 kPa.

$$\begin{aligned} Q &= 20.53 \psi^{-1.050}, & r^2 &= 0.996; \\ K &= 3.03 \cdot 10^{-4} \psi^{-2.989}, & r^2 &= 0.985; \\ K &= 5.40 \cdot 10^{-8} \theta^{2.825}, & r^2 &= 0.973. \end{aligned}$$

TABLE VI  
HYDRAULIC CONDUCTIVITY  
OF SOLID TUFF AS A  
FUNCTION OF MATRIC POTENTIAL

Matric Potential (-kPa)	Saturation Ratio	Calculated Conductivity $K_{sc} (\text{m s}^{-1})$	Corrected Conductivity $K (\text{m s}^{-1})$
780	0.017	$9.8 \cdot 10^{-11}$	$1.4 \cdot 10^{-12}$
200	0.083	$1.6 \cdot 10^{-9}$	$2.3 \cdot 10^{-11}$
115	0.150	$9.1 \cdot 10^{-9}$	$1.3 \cdot 10^{-10}$
82	0.217	$3.0 \cdot 10^{-8}$	$4.3 \cdot 10^{-10}$
60	0.283	$7.7 \cdot 10^{-8}$	$1.1 \cdot 10^{-9}$
48	0.350	$1.6 \cdot 10^{-7}$	$2.3 \cdot 10^{-9}$
41	0.417	$3.2 \cdot 10^{-7}$	$4.5 \cdot 10^{-9}$
36	0.483	$5.4 \cdot 10^{-7}$	$7.7 \cdot 10^{-9}$
33	0.550	$8.5 \cdot 10^{-7}$	$1.2 \cdot 10^{-8}$
29	0.617	$1.3 \cdot 10^{-6}$	$1.8 \cdot 10^{-8}$
25	0.683	$2.0 \cdot 10^{-6}$	$2.8 \cdot 10^{-8}$
20	0.750	$2.8 \cdot 10^{-6}$	$4.0 \cdot 10^{-8}$
13	0.817	$4.2 \cdot 10^{-6}$	$6.0 \cdot 10^{-8}$
1	0.883	$6.5 \cdot 10^{-5}$	$9.2 \cdot 10^{-8}$

The tight power fit existing between saturation ratio and matric potential, hydraulic conductivity and matric potential, and, finally, hydraulic conductivity and saturation ratio are demonstrated by the very high coefficients of determination ( $r^2$ ) existing below  $-15$  kPa. Moisture characteristic curves for crushed and solid tuff are drawn in Fig. 9.

Graphic comparisons between the *calculated* hydraulic conductivities of solid tuff and the *measured* hydraulic conductivities of crushed tuff as a function of matric potential and saturation ratio are shown in Figs. 10 and 11.

## VII. HYDROLOGIC MONITORING

### A. Parameters Influencing Neutron Probe Readings

Often moisture must be measured with a neutron probe in access holes whose liner materials or diameters differ substantially from those the manufacturer considers ideal. The calibration chart accompanying the Troxler probe tested was valid for a thin-walled aluminum access pipe of 0.051 m outside diameter.

Computing soil moisture content with a neutron probe requires use of additional calibration curves that consider the hole diameter as well as the thermal neutron capture cross section of the hole liner, if those parameters are going to differ from those proposed by the manufacturer of the probe. The influence of steel, polyvinyl chloride, and aluminum casings that fit 0.051- to 0.102-m hole diameters was determined by comparison with neutron probe readings in uncased holes of corresponding diameters. Eccentricity of probe location was considered a potentially significant variable. The experiment was run in disturbed Bandelier tuff with an average dry density of  $1350 \text{ kg m}^{-3}$  and moisture content of 3.8 to 26.7% by volume. The casing material and hole diameter influenced the probe readings significantly, whereas eccentric location of the probe did not. Regression analyses showed an almost perfect inverse linear correlation between hole diameter and count rate (Abeele, October 1979).

### B. Prior Measurements

Moisture relationships of the Bandelier tuff during the late 1950s and early 1960s (Abrahams, 1961) were extensively studied. Physical properties (density, porosity, etc.) and hydrologic properties

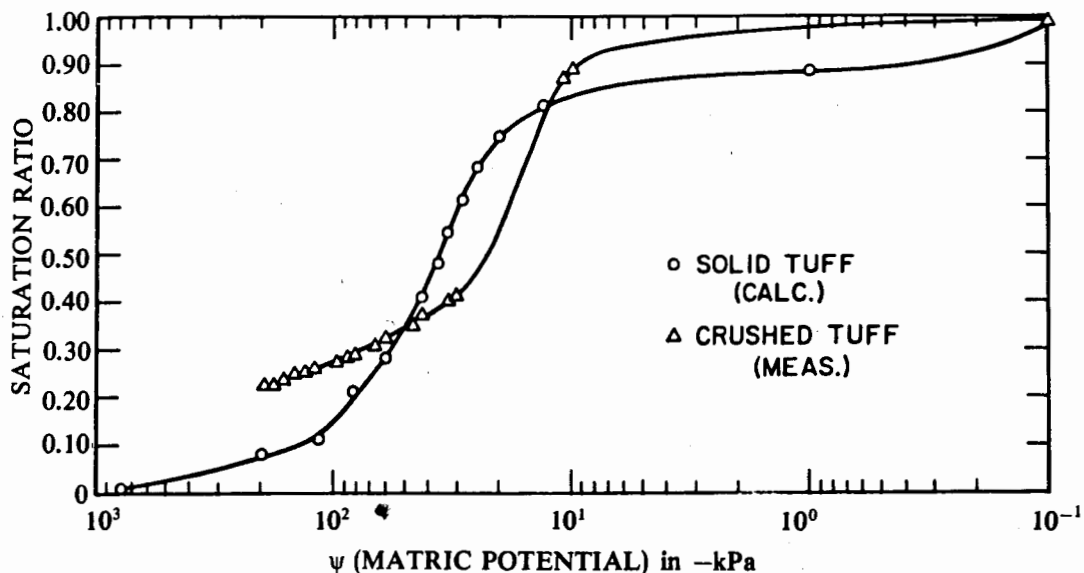


Fig. 9. Saturation ratio as a function of matric potential (moisture characteristic curves).

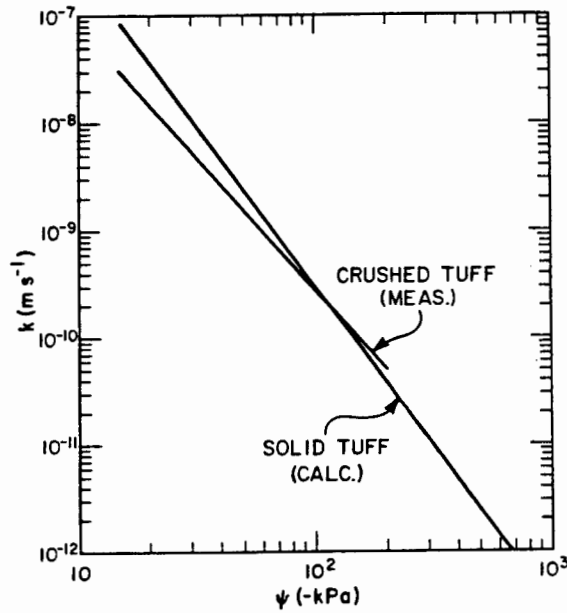


Fig. 10. Hydraulic conductivity as a function of matric potential.

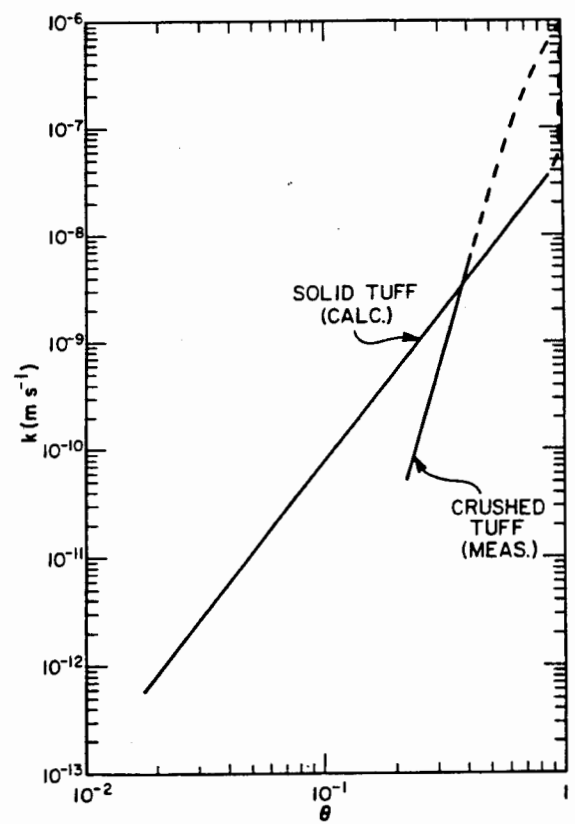


Fig. 11. Hydraulic conductivity as a function of saturation ratio.

(permeabilities, moisture tension curves, etc.) were measured on samples of tuff, and field experiments were conducted to investigate infiltration under high moisture conditions.

Data were also collected on the natural moisture conditions in the tuff, showing values of 5 to 10% by volume below a depth of a few meters. Variable amounts of precipitation infiltrate and percolate through the tuff or soil. Where the soil cover has not been disturbed, little if any water from precipitation infiltrates the underlying tuff (Purtymun and Kennedy, 1971). Where the soil cover was disturbed, as in the waste disposal areas, the moisture content of the tuff indicates a much higher degree of infiltration than the one that might have been implied by the moisture content fluctuations found in the undisturbed tuff.

Tests of precipitation infiltration in the disturbed tuff composing the pit overburden showed that moisture from a single storm may reach depths nearing 2 m, but in subsequent weeks is returned to the atmosphere by evaporation (Purtymun and Kennedy, 1971). Data on moisture contents of the tuff are presented in Table VII and Figs. 12 and 13.

TABLE VII  
MOISTURE CONTENT OF BANDELIER TUFF<sup>a</sup>

Site	Depth (m)	Moisture Content (% by Vol.)
TA-49	0-30	2.1
	30-80	1.2
TA-33	0-2	16
	2-4	5.3
TA-3	0-3	16.5
	3-6	10.4

<sup>a</sup>(From Abrahams, 1963)

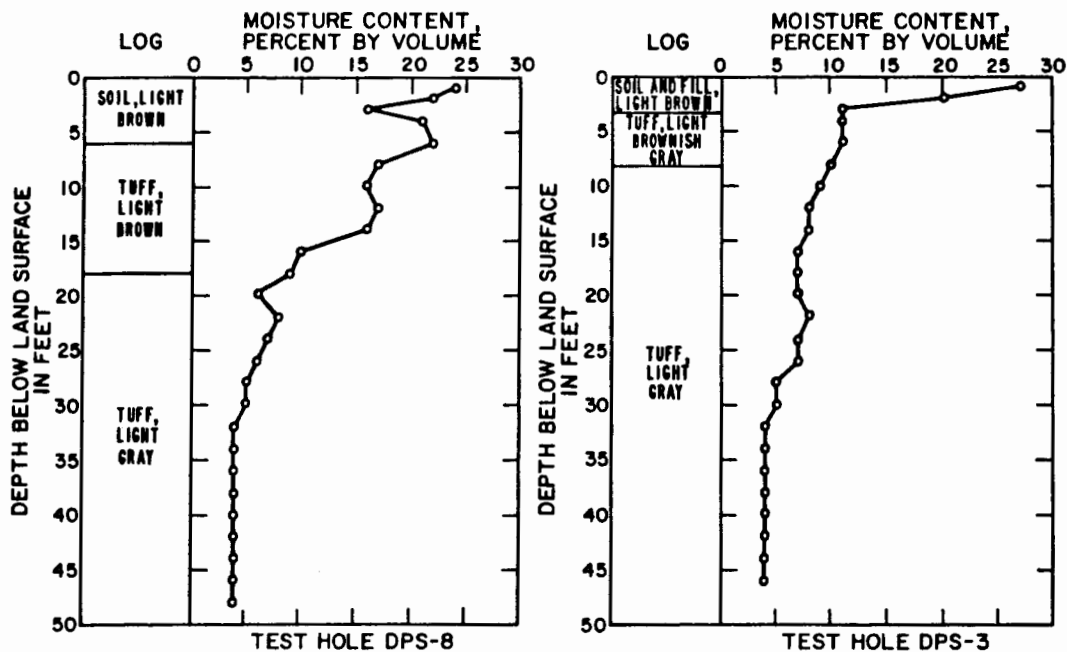


Fig. 12. Moisture distributions at TA-49 (Abrahams, Weir & Purtymun, 1961).

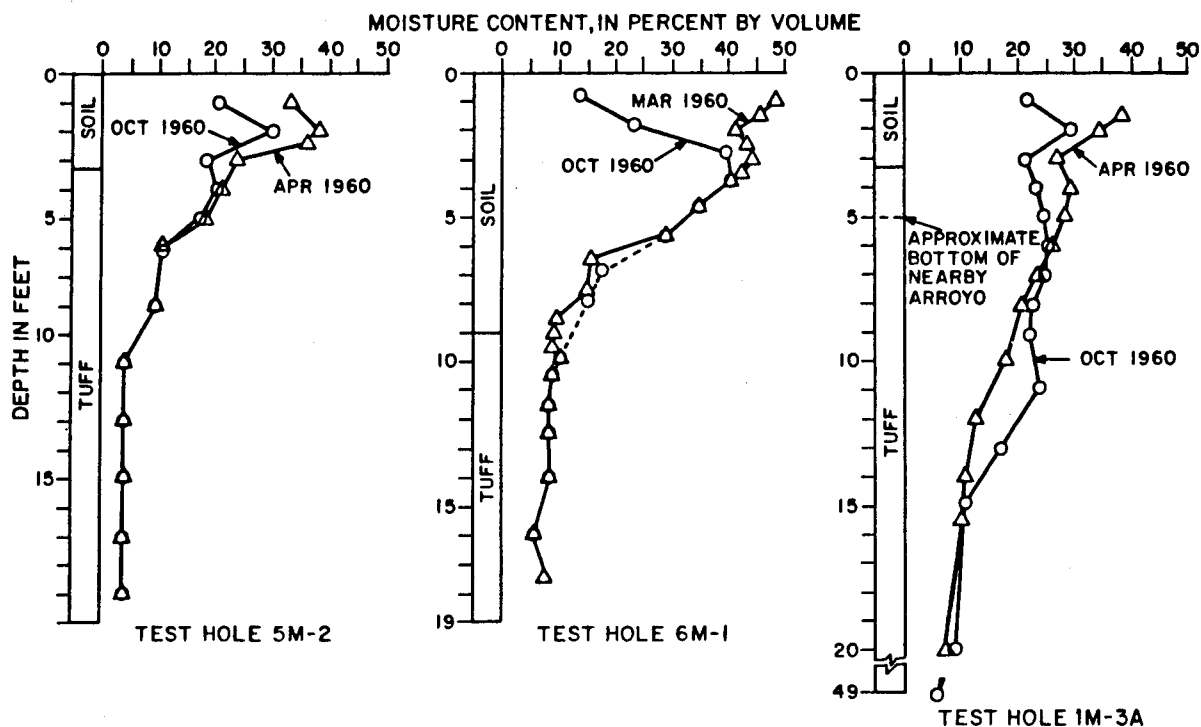


Fig. 13. Moisture distributions in Bandelier Tuff near TA-21 (Purtymun & Kennedy, 1966).

### C. Current Monitoring

1. **History.** During the early 1970s there was renewed interest in establishing the dynamics of water and radionuclide movement within the Los Alamos radioactive waste disposal sites. A series of moisture access holes was drilled to allow monitoring of moisture depth distributions over a long time period. These investigations were also intended to establish the best means of installing access holes, optimum locations and measurement schedules, and the number of monitoring points required.

Measurements of the moisture content of solid and crushed tuff were made using a neutron moisture gauge (Abeele, October 1979). A description of the history and current status of the monitoring holes is presented in Appendix A. A summary of the measurement history is presented in Table VIII. The measurement data for these holes are on file with the Environmental Sciences Group, LS-6.

#### 2. Data Discussion.

*a. Area C.* Four access holes were drilled in Area C in 1978. They are cased with aluminum tubing to about 1 m below the surface, below which the hole is open with an original diameter of about 8.5 cm. Geophysical logs of these holes revealed significant caving, to diameters of 25 cm in some cases, associated with low density zones such as pumice beds.

A summary of data from two of the holes (CP2-1, CP6-1), representative of all four, is presented in Figs. 14 and 15. Moisture contents below 30 m average between 6 and 7% by volume for CP2-1 and between 8 and 10% for CP6-1 and show no significant net gradient. Localized variations in moisture contents are probably caused by differences in the moisture tension relationships of various flow units. Moisture contents are expressed in per cent by volume or more often as Moisture Ratio by Volume (MRV).

A fifth hole, identified as TA52-1, was drilled just outside the perimeter fence at Area C, to obtain data on moisture conditions beneath undisturbed areas.

TABLE VIII

HISTORY AND CURRENT STATUS AT MONITORING HOLES

Hole	Original Depth (m)	Casing	Nominal Diam. (mm)	Current Status <sup>a</sup>
GP1-1	5.5	PVC	51	Active
GP1-2	3.5	PVC PVC & Steel, to 1 m	51 51	Active Active
GS50-1	15	Open below to 2 m	102	Inactive
GP7-1	40	PVC	102	Inactive

<sup>a</sup>Status Types:

Active = Part of measurement net

Inactive = No measurement for > 2 yr (plugged/abandoned)

MONTHS 8,10,11 = 1978  
 MONTHS 13,14,15,17,18 = 1979  
 MONTHS 19,20,21,22,23 = 1979

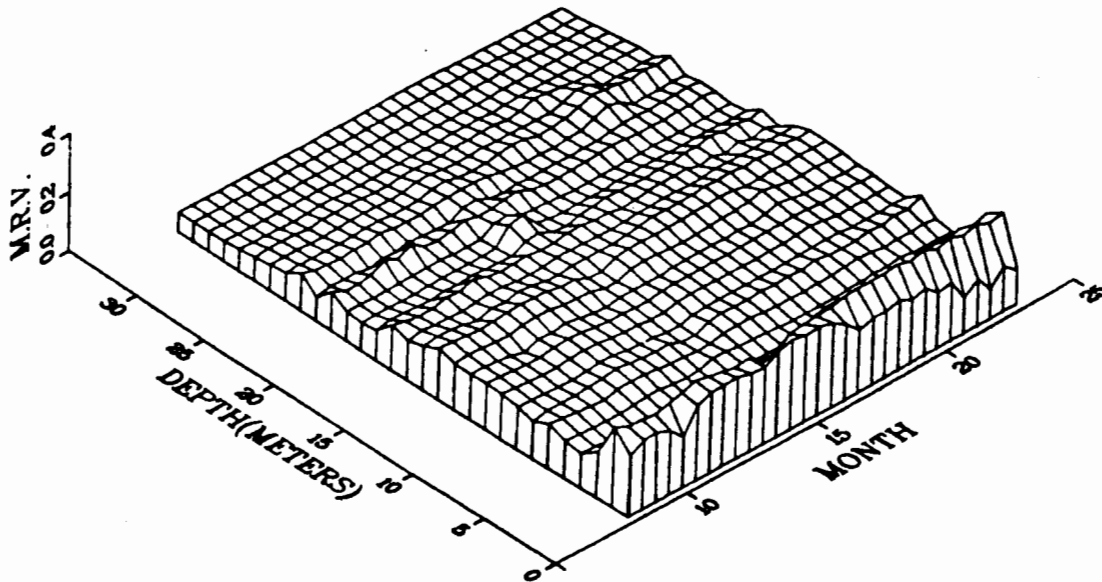


Fig. 14. Moisture Hole CP2-1.

MONTHS 8,10,11,12 = 1978  
MONTHS 13,14,15,17,18 = 1979  
MONTHS 19,20,21,22,23 = 1979

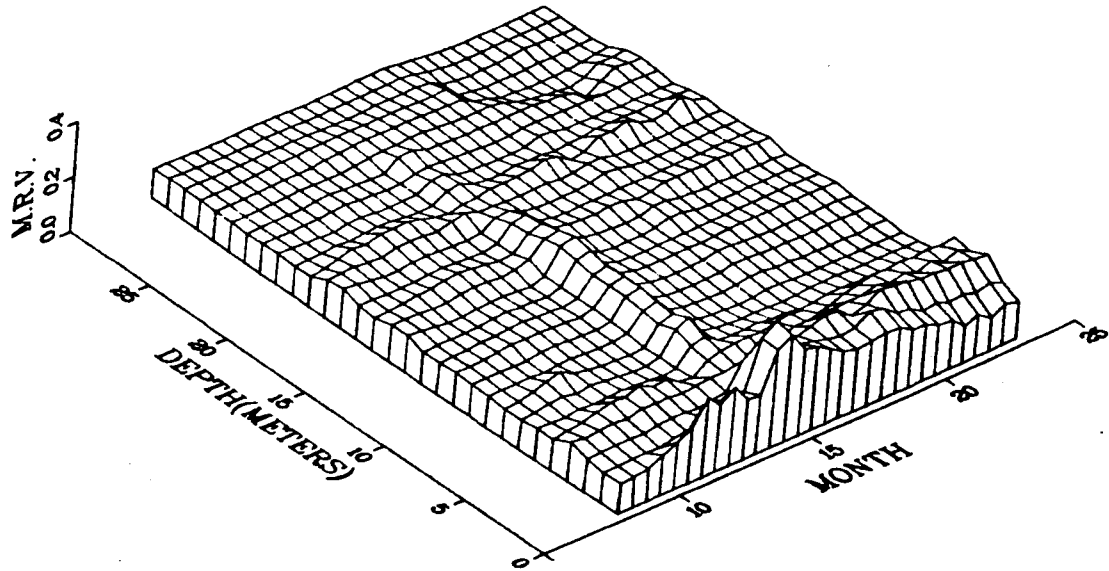


Fig. 15. Moisture Hole CP6-1.

*b. Area G.* Four holes were drilled in fill material overlying waste disposal pits (GP2-1, GP2-2, GP1-1, GP1-2) and cased with 5-cm PVC pipe. The former two were too shallow to obtain any significant data on depth distributions of soil moisture. Data from GP1-1, the deeper of the remaining two, is presented in Fig. 16. The data show significant seasonal fluctuations in moisture content to a depth of about 4 m, with a downward moisture flux below that depth. This flux, if it continues, will eventually raise the moisture content of the waste pit to a level above that of the surrounding undisturbed tuff, implying a gradual diffusion of moisture out of the waste pit. This condition results, in part, from the higher hydraulic conductivity of crushed tuff at high water content, compared with solid tuff. Changes in surface topography that reduced runoff are also partly responsible for disturbance of the natural moisture regime.

Six holes (GS50-1 to GS50-6) were drilled in solid tuff within the shaft disposal field. The holes are cased with steel pipe to a depth of about one meter, with an open hole of about 10.5 cm diameter below that depth. The holes were designed, in part, to detect possible moisture gradients away from Shaft 50, a source of tritium release from the shaft field (Wheeler and Warren, 1975). Data from two of these holes (GS50-3, GS50-5) are presented in Figs. 17 and 18. The data show seasonal fluctuations in moisture content in the upper 4 m, with no significant changes below that depth. The presence of stable "bulges" in the moisture content, underlain by regions of essentially constant moisture content, suggest that moisture is being held in the tuff, with no significant changes in moisture content during the measurement period. These bulges result, most probably, from variations in the moisture tension relationships of the tuff. For example, the bottom of the upper bulge coincides with the presence of a low-density pumice bed, a unit which would be expected to impede the downward flow of moisture. The moisture depth distributions show substantial stability over time, suggesting essentially steady-state conditions. No significant moisture gradients away from the shaft can be identified.

MONTHS 4,5,6,7,8,9,10,11,12 = 1978  
MONTHS 13,14,15,16,17,18 = 1979  
MONTHS 20,21,22,23,24 = 1979

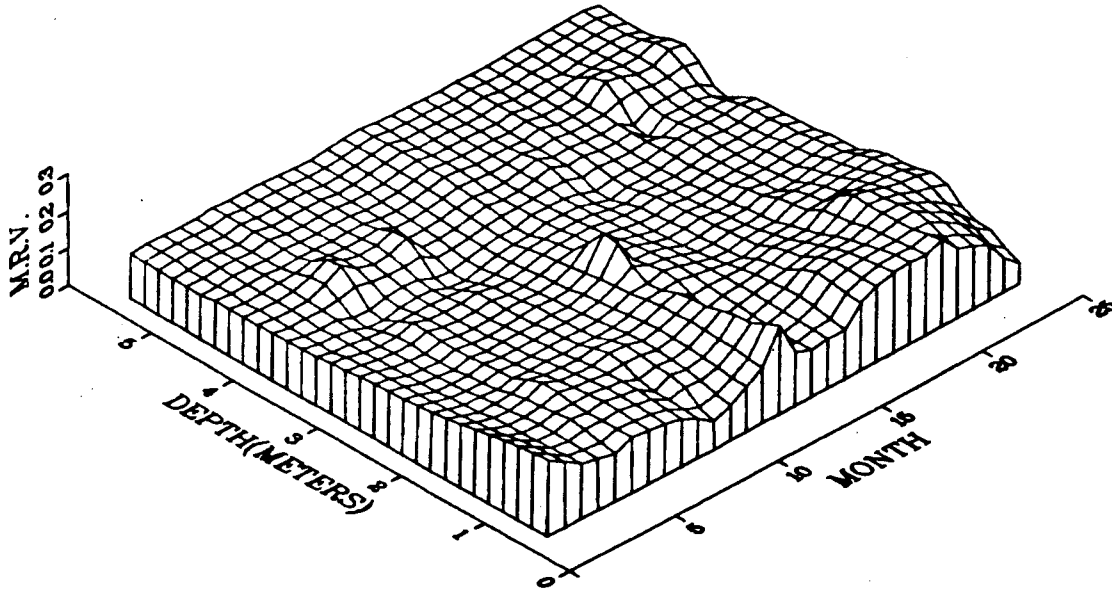


Fig. 16. Moisture Hole GPI-1.

MONTHS 4,5,6,7,8,9,10,11,12 = 1978  
MONTHS 13,14,15,16,17,18 = 1979  
MONTHS 19,20,21,22,23,24 = 1979

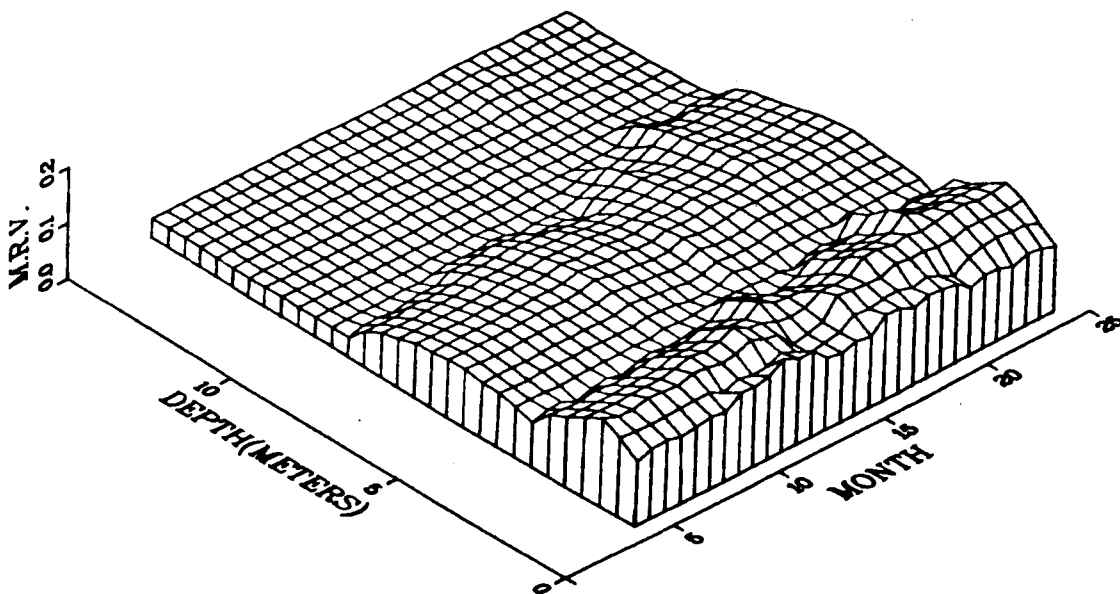


Fig. 17. Moisture Hole GS50-3.

MONTHS 4,5,6,7,8,9,10,11,12 = 1978  
 MONTHS 13,14,15,16,17,18 = 1979  
 MONTHS 19,20,21,22,23,24 = 1979

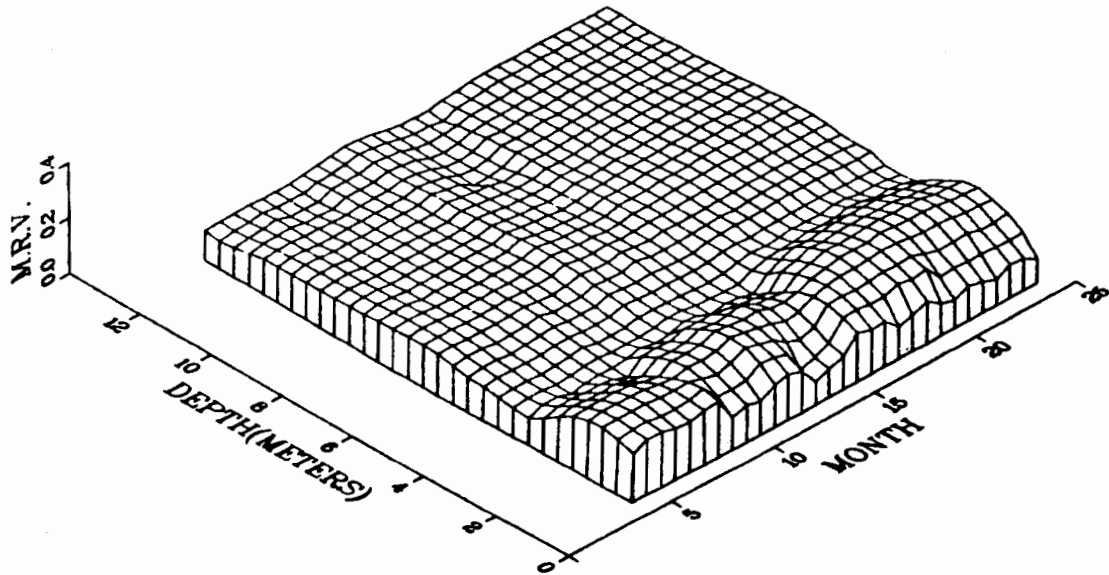


Fig. 18. Moisture Hole GS50-5.

Access holes were drilled in the bottom of Pits 7, 8, and 24 before backfilling was completed. Casings were extended to the surface before or during the filling process. All of the casings in Pit 8 were bent or broken beyond use during the filling process. Protective frameworks were constructed around the casings in Pits 7 and 24. However, several of these casings were also bent or broken beyond use during the filling process. Geophysical logs of two of these holes show extreme density variations (suggesting open voids) around the casings in GP7-2 and GP7-3, as well as breaks in both casings.

Moisture readings in the cased portions of the holes had been discontinued before these logs were collected because of the apparent meaningless nature of the data. Extreme variations in hole diameter and density are known to affect the readings (Abeele, October 1979). Data for Hole GP7-2 in the bottom of Pit 7 are presented in Fig. 19. The constantly low moisture distribution with depth, with the only exception occurring at the bottom of the pit (in the upper layers), suggests steady-state conditions with downward moisture flux due only to gravitational forces. Quantitative evaluation of this moisture flux suggests a downward rate of  $10^{-11} \text{ m s}^{-1}$  (0.3 mm per year).

One hole, GP26-1, was drilled in an undisturbed area. The hole is cased with 5-cm plastic pipe for the upper 0.5 m, below which the hole is open with an original diameter of about 10.5 cm. Geophysical logs indicate that some slumping of the sidewall has occurred, even though the hole was drilled only about 6 months before the logging. However, after the hole was constructed, pits were excavated near by, and the hole may provide data on the possible disturbance of the natural moisture regime by these pits. Only a limited amount of data have been collected from this hole and are not presented here.

*c. Area F.* A hole was drilled in the upper 0.5 m and cased with a 5-cm plastic pipe. The remainder of the hole was open, with a diameter of about 10.5 cm. The hole was intended to develop data on moisture contents of the tuff in a zone of relatively high precipitation, compared with Area C or Area G. However, insufficient data have been collected to date to make any such evaluations.

MONTHS 1,2,3,4,5,6 = 1978  
 MONTHS 7,8,9,10,11,12 = 1978  
 MONTHS 13,14,15,17,18 = 1979  
 MONTHS 19,20,21,22,23 = 1979

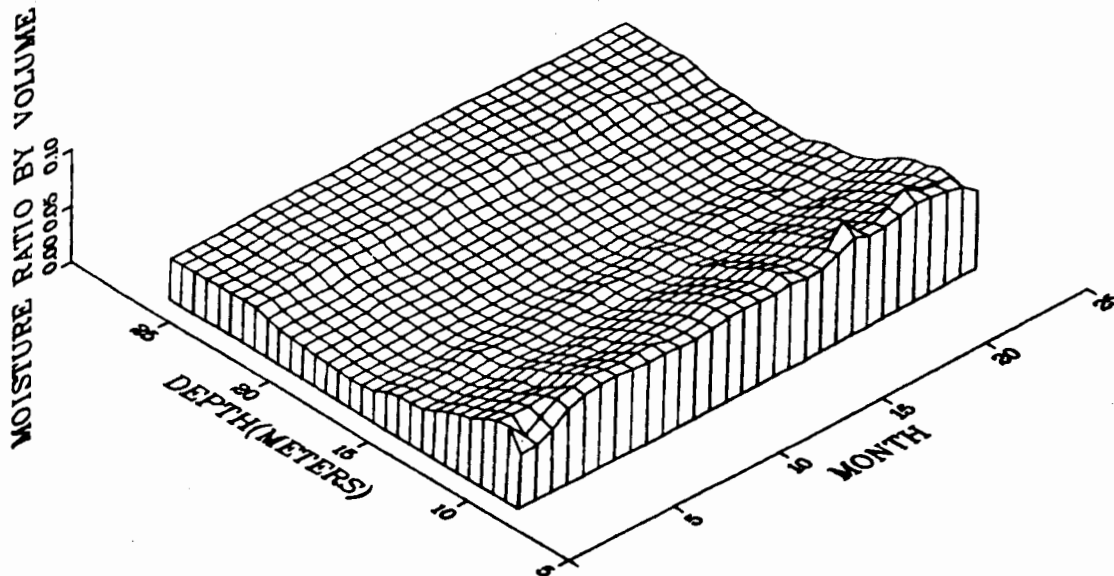


Fig. 19. Moisture Hole GP7-2.

*d. TA-51.* An access hole was drilled in an undisturbed area within TA-51 to obtain data on undisturbed moisture contents at a location midway between Areas C and G. Coincidentally, the area adjacent to the hole has been selected as the site of an experimental waste burial site. Although only limited data have been collected, background information on conditions in the area before construction at the adjacent site may be provided.

**3. Geophysical Logging.** Natural gamma, density (using gamma-gamma), neutron, and caliper logs were obtained for all of the holes described above. The caving of the holes in low-density zones has been discussed. The logs showed significant density variations with depth (see Section IX: Stratigraphic Controls on Flow). These density variations result from porosity changes in the tuff because of differing degrees of induration and material composition. Such variations have a significant effect on hydraulic properties, suggesting that detailed modeling of moisture flow will require extensive measurement of these properties for the various units. Conversely, the data collected during the past 6 years suggest that steady-state conditions prevail in all but near-surface portions of the tuff, and relatively simplistic analyses of the moisture flux may prove adequate to evaluate the potential for moisture and radionuclide flux within the disposal site.

The gamma logs proved useful in identifying unit contacts because of changes in natural radiation that occurred in the various units. These supported unit boundary identifications made with the density logs. The neutron logs, used primarily to determine porosity in saturated material, proved of little value for moisture content determinations. The particular probe used has a relatively long spacing between the source and detector (30 cm). Differences in chloride content of various units (determined by sample analysis) appear to result in differential neutron absorption. These differences are unrelated to moisture contents.

**4. Justification for Converting to "Inactive."** After extensive inspection of the data gathered in the existing monitoring holes, it was concluded that monitoring of several access holes should be eliminated.

This decision was based on similar moisture characteristics that seemed to prevail in adjacent monitoring holes (S50, P1, and P2). The decision concerning the P7 monitoring holes was more difficult because the part that goes through the pit is cased with PVC, whereas the part beneath the pit is uncased so that two different calibration curves had to be applied. An Analysis of Variance applied to the layer of soil that was backfilled in the pit around the monitoring hole showed a significant difference in moisture readings between monitoring holes. This could be caused by the presence of materials other than inorganic soils, or interference from the surrounding waste that could create preferential pathways for moisture into the soil around the monitoring holes because of successive layers of extremely permeable and impermeable waste material. These fluctuating moisture readings were therefore judged to be quite unreliable. The Analysis of Variance showed that there was no significant difference in undisturbed tuff moisture between P7-1 and P7-2 below 9 m.

As a consequence, and because shallow hole P2-1 was to be covered, monitoring of holes S50-1, S50-3, S50-5, P1-1, and P1-2 was retained. The monitoring of P7-1 and P7-3 was also continued below 9 m. P7-1 was chosen over P7-2 because of its greater depth.

## VIII. TRITIUM MIGRATION

### A. Tritiated Water in Soils

Radionuclides disposed of at the Los Alamos National Laboratory include significant amounts of transuranics (mostly plutonium and americium), uranium, fission products, activation products, and tritium. All investigations of the radioactive waste disposal areas revealed that, with the exception of tritium, no migration of these radionuclides has been detectable. Because of the high mobility of tritium in biological systems, there is a legitimate need to define and minimize the quantities of this radionuclide entering the environment from disposal areas (Wheeler et al., 1975). Migration of tritium from its disposal site was detected as early as 1970, although dissolution and subsequent migration of solid radionuclides in the disposal area is minimal. This has been verified continually by analysis of innumerable samples collected during the excavation of additional shafts in the disposal areas. Tritium, on the other hand, occurring principally as tritiated water, is nearly as free to move as water itself. Small quantities of tritium gas, disposed of by burial, convert very quickly to HTO on exposure to soil oxygen and moisture.

Before mid-1958, all tritium-containing wastes were disposed of by burial with other wastes in disposal pits. Since that time and until November 1973, unlined shafts, 8 to 20 m deep and possessing a diameter of 0.6 to 1.8 m, were used. Since November 1973, the walls and bottom of the disposal shafts for tritium waste have been coated with a 1- to 2-cm layer of asphalt. The primary motivation was an attempt to seal the many fractures in the tuff walls of the shaft, because it was believed that such fractures provided possible pathways for tritium migration (Wheeler et al., 1975). A study had previously shown that unlined tritium shafts were significant sources of soil contamination (Purtymun, 1973). In that study, it is shown that around an unlined shaft (number 13, Area G, Technical Area 54 on the Mesita del Buey), the tritium concentration in the surrounding tuff increased to a maximum between depths of 3 to 10 m and then decreased again with depth. Irregularities in the isotritium contours are seemingly influenced by the presence of open joints in the tuff, which provide for a much more rapid means of migration in the vapor phase. Close but irregular isotritium contours or high tritium gradients are to be found between the source (shaft) and an eventual transversal joint. The contours are elongated to the west of the shaft, indicating regions where either a radial joint was present or the outward (upward) movement of tritium was inhibited. High tritium gradients would consequently be an indication of swift, uninhibited aeration of tritium. A close and complete set of isotritium contour lines, which deserved close scrutiny, have been chosen along a southwest axis. The presence of tritium radioactivity decreases logarithmically with distance from the shaft. Table IX indicates the rate of decrease at various depths of radioactivity as a function of distance from the shaft. There were as many as seven contour lines intersecting the southwest

**TABLE IX**  
**DECREASE IN RADIOACTIVITY NEAR SHAFT 13**  
**AS A FUNCTION OF DISTANCE FROM THE SHAFT**  
**ALONG A S-W AXIS**

Depth (m)	Rate of Decrease (Bq m <sup>-3</sup> )	Coefficient of Correlation
3.75	$A = 3.1 \cdot 10^9 - 1.01 \cdot 10^9 \ln d$	$r = 0.96$
6.75	$A = 1.24 \cdot 10^{10} - 5.27 \cdot 10^9 \ln d$	$r = 0.97$
9.75	$A = 2.87 \cdot 10^9 - 1.04 \cdot 10^9 \ln d$	$r = 0.98$
12.75	$A = 1.23 \cdot 10^9 - 5.28 \cdot 10^8 \ln d$	$r = 0.96$

axis. The radioactivity is measured in Becquerels per cubic meter of water. Most interestingly, a vertical plane along the shaft axis showed that the maximum tritium concentration was located near the bottom of the shaft with the radioactivity decreasing upward according to  $A = 1.11 \cdot 10^{10} - 6 \cdot 10^9 \ln d$  and  $r = 0.97$ . The similarity between the rate of decrease in radioactivity as a function of distance is striking along the vertical and horizontal planes! The closest match is between the horizontal rate of decrease as a function of distance from the shaft at 6.75-m depth and the vertical rate of decrease upward as a function of distance from the bottom of the shaft.

Shafts 50 and 59, also located in Area G, Technical Area 54 on the Mesita del Buey, have received tritium contaminated waste since 1973. Approximately the same time period elapsed between the placement of the waste and the collection of samples in shafts 50 and 59 as in shaft 13. Both shafts 50 and 59 were asphalt lined and asphalt containment was applied to the packaging of wastes placed in the shafts. Yet, on a percentage basis, significantly more tritium has migrated out of shafts where asphalt containment was used than from shafts where no asphalt was applied. Undoubtedly many factors contribute to this difference, including different waste forms and packaging before asphaltting, variabilities in permeability of the tuff, and differences in the size and number of fractures intersected by the various shafts. However, the asphaltting was intended to counteract and override these variabilities. It is concluded that the asphaltting techniques, as applied in the past, did not significantly reduce the migration of tritium away from the disposal shafts. The shafts also appear to serve as a moisture source to the tuff, particularly at depth (Wheeler et al., 1975). This is probably because of the entrance of precipitation into the shafts during and between waste deliveries and before they are sealed off. The asphalted bottom serves as an inhibitor to the flow of moisture out of the shaft and this moisture in turn increases the total amount of water vapor to be diffused out of the shaft after its closure.

In this case also, tritium activity decreases logarithmically with distance from the shaft. Table X indicates, at two different depths, the rate of decrease of radioactivity as a function of distance from shafts 50 and 59. The fastest rate of decrease away from shaft 50 is along a SSW axis, while it seems fastest along the eastern axis originating at shaft 59. However, the tritium data are incomplete along the eastern axis, so that the next steepest gradient, along the northern axis, was chosen for analysis. For the tuff surrounding shafts 50 and 59, the radioactivity was measured using as basis a unit volume of tuff instead of water, as was used for the analyses surrounding shaft 13. Based on this fact, the constants in the regression equations should be quite a bit higher for shaft 13 for equal degrees of contamination. Since this is barely the case, it can be concluded that tritium contamination is substantially higher around shafts 50 and 59. The rates of decrease as a function of distance from the shaft are strikingly similar in both cases!

Because the preceding studies revealed that the asphalt was not significantly retarding tritium migration away from disposal shafts, a decision was made by the Waste Management Operations Group (H-7) to implement more rigorous packaging procedures involving the use of asphalt for tritium containing wastes. Asphalt coating of the shaft itself was eliminated.

**TABLE X**  
**DECREASE IN RADIOACTIVITY NEAR SHAFTS 50 AND 59**  
**AS A FUNCTION OF DISTANCE FROM THE SHAFT**

Shaft	Axis	Depth (m)	Rate of Decrease (Bq m <sup>-3</sup> )	Coefficient of Correlation
50	SSW	3.75	$A = 1.01 \cdot 10^9 \cdot 6.09 \cdot 10^9 \text{Ind}$	$r = 0.98$
50	SSW	6.75	$A = 1.21 \cdot 10^9 \cdot 5.61 \cdot 10^9 \text{Ind}$	$r = 0.94$
59	N	3.75	$A = 1.03 \cdot 10^9 \cdot 6.06 \cdot 10^9 \text{Ind}$	$r = 0.96$
59	N	6.75	$A = 1.18 \cdot 10^9 \cdot 5.73 \cdot 10^9 \text{Ind}$	$r = 0.96$

To test the effectiveness of the new procedures, the new disposal shaft, No. 150, was located in an area where no prior tritium disposals had occurred. The extent of tritium migration into the tuff surrounding the shaft could then be related directly to the contents of the shaft. Disposal shaft 150 was drilled in the spring of 1976, with the first disposal occurring on 12 May 1976. In the winter of 1977, after more than  $1 \cdot 10^{15}$  Bq (30 000 curies) of tritium had been disposed to the shaft, nine sampling holes were augered around the shaft. The samples were processed to remove the contained water, and the water was analyzed for tritium. The sampling holes were provided with surface casings and then sealed. Subsequently, in the fall of 1979, samples of the water vapor in the access holes were collected using silica gel as an absorbing medium. Water was distilled from the gel and analyzed for tritium. Also, the moisture content of the tuff surrounding the access holes was determined using a neutron moisture probe. The average water content in the tuff surrounding the shaft was about 4% by volume. This value agrees well with other measurements made in the area.

This latest study shows a release of 0.5 to 0.7% of the tritium in the shaft to the surrounding tuff vs an estimated 0.3 to 0.6% in the two previous cases. Thus, no substantial improvement in tritium containment was obtained by the new procedures. It is difficult to establish whether the packaging procedures themselves were inadequate, or the quality control on the procedures was inadequate.

Release of tritium to the surrounding tuff is not a significant health hazard; however, as the inventory of tritium in the disposal site continues to grow, improved methods will be necessary to provide additional containment. The results of this study have led to the design of further improvements in the techniques for tritium disposal. Sealed steel liners will be coated with asphalt and placed inside vertical shafts.

#### **B. Emanation of Tritiated Water**

1. The gradual mixture of tritiated water with natural soil moisture and subsequent evaporation of that water from the soil to the atmosphere results in a gaseous release from the burial ground. One study involved measuring the atmospheric release of tritiated water from Burial Pit 1, Area G. Soil borings in cover material overlying the waste showed tritium concentrations increasing from  $7.4 \cdot 10^7$  Bq m<sup>-3</sup> (2000 pCi/ml) of soil moisture at 15 cm to  $4.6 \cdot 10^9$  Bq m<sup>-3</sup> (125 000 pCi/ml) at 3.5 m. This gradient suggested an upward diffusion of tritiated water from the waste (at a depth below 3.5 m) to the surface soils. This tritiated water mixes with meteoritic soil moisture and is evaporated. The experimental measurements were designed to quantify the tritium flux and to establish the controlling factors.

Samples of evaporated soil moisture were collected on silica gel in covered sieves. Collection was at night, or on cloudy days, to reduce thermally induced lateral moisture fluxes. The average moisture flux and tritium flux were determined for the collection period. Atmospheric boundary layer data (vapor pressure) were collected. Soil moisture contents were measured from 0.5 to 1.5 m using a neutron moisture probe.

Correlations were made between tritiated water flux, (as dependent variable) and the various atmospheric and soil conditions. No significant correlation could be demonstrated between atmospheric conditions and tritiated water flux. The best correlation was obtained using soil moisture contents at 0.4 m and the soil moisture vapor pressure at 0.4 m. Measured tritiated water fluxes varied from  $2 \cdot 10^{-3} \text{ Bq m}^{-2} \text{ s}^{-1}$  ( $0.005 \mu\text{Ci m}^{-2} \text{ day}^{-1}$ ) to  $2 \cdot 10^{-1} \text{ Bq m}^{-2} \text{ s}^{-1}$  ( $0.44 \mu\text{Ci m}^{-2} \text{ day}^{-1}$ ). The actual surface area contributing to this flux was not established, but, as previously mentioned, measurements of the tritium distribution in the soil suggest that only a portion of this particular pit is contributing. Pit dimensions are approximately 30 m by 200 m ( $6 \cdot 10^3 \text{ m}^2$ ). If the entire pit were a source at the observed rate, atmospheric releases would range from  $13 \text{ Bq s}^{-1}$  to  $1.1 \cdot 10^3 \text{ Bq s}^{-1}$  ( $30 \mu\text{Ci day}^{-1}$  to  $2640 \mu\text{Ci day}^{-1}$ ) during the measurement period. Because only some fraction of the total pit is actually contributing to tritium releases, the actual tritium released is less than this amount.

If the soil vapor pressure at 0.4 m is used as an independent variable together with the moisture ratio by volume at 0.4 m, measured with the neutron probe, a correlation coefficient of 0.7947 is obtained with tritiated water vapor aeration as the dependent variable. This coefficient of correlation is significant at the 1% level of confidence. Whether this highly significant coefficient of correlation is an indication of cause and effect relationship is somewhat arguable since temperature gradient, for example, could be the only reason for the existence of a vapor-pressure gradient. However, the relationship between temperature, moisture ratio by volume, and tritiated water aeration was not as good as the one between vapor pressure, moisture ratio by volume, and tritiated water aeration. The multiple correlation coefficient in that case was 0.7128. The difference is caused by the nonlinear relationship between temperature and saturated vapor pressure, but the lower values obtained using temperature as an independent variable do not exclude the fact that temperature *itself* is a cause for higher tritiated water vapor aeration. However, the higher correlation coefficients obtained using measurements taken at greater depths seem to indicate that liquid water flow is a more important factor in tritium aeration than vapor flow. This conclusion was reached because moisture content was increasing significantly with depth over the range considered and it is a known fact that liquid flow becomes more and more prevalent as the moisture content increases.

The addition of the atmospheric vapor pressure as an independent variable did not improve the multiple correlation coefficient. This is caused by the very nature of the experiment because the silica gel created a vapor pressure that was essentially zero in all cases at the soil-atmosphere interface. The moisture content was found to be maximum at 1 m; the loss of moisture in the upper meter, after correction for precipitation, was 9.95 mm between the 1st and 12th of June. This was measured using the neutron probe.

Based on the discontinuous nightly measurements using the silica-gel-filled sieve, and through interpolation, a total of 10.69 mm was predicted. The two above values seem to agree fairly well. The difference could be because of instrumental error, or higher evaporation induced by the presence of silica gel, or both.

2. Two sieves filled with silica gel and covered by a heavy aluminum plate were placed at spots equidistant from shafts 50 and 59, one at 6 m and the other at 10 m from the shafts, respectively. The activity measurements taken in February amounted to a tritiated water flux of  $0.82 \text{ Bq s}^{-1} \text{ m}^{-2}$  ( $2.22 \cdot 10^{-5} \mu\text{Ci s}^{-1} \text{ m}^{-2}$ ) and  $0.22 \text{ Bq s}^{-1} \text{ m}^{-2}$  ( $6 \cdot 10^{-6} \mu\text{Ci s}^{-1} \text{ m}^{-2}$ ), respectively.

3. Emanation of tritiated water was measured along 3 axes, A, B, C,  $120^\circ$  apart, around GS-150. The measured average concentration read  $6.1 \cdot 10^8 \text{ Bq m}^{-3}$  of soil water ( $1.65 \cdot 10^4 \text{ nCi/l}$ ) for an area including  $113.10 \text{ m}^2$ . Because the evaporation rate was averaging  $7.75 \cdot 10^{-9} \text{ m s}^{-1}$ , the total release of tritiated water was:  $6.1 \cdot 10^8 \text{ Bq m}^{-3} \times 7.75 \cdot 10^{-9} \text{ m s}^{-1} = 4.75 \text{ Bq m}^{-2} \text{ s}^{-1}$  ( $1.11 \cdot 10^4 \text{ nCi m}^{-2} \text{ day}^{-1}$ ), or within the area under consideration (6 m radius):  $535 \text{ Bq s}^{-1}$  ( $1.25 \text{ mCi day}^{-1}$ ). Along each of the three axes, the rate of tritium emanation drops off with distance from the shaft according to a power function.

With  $d$ , the distance, expressed in meters and  $E$ , the tritiated water emanation, expressed in  $\text{Bq m}^{-2} \text{ s}^{-1}$ , the regression analysis for the three different axes yields

$$\begin{aligned} E &= 95.5 d^{-4.7546}, & \text{with } r &= 0.9902; \\ E &= 104 d^{-4.4050}, & \text{with } r &= 0.9972; \text{ and} \\ E &= 133 d^{-5.0313}, & \text{with } r &= 0.9881. \end{aligned}$$

The average regression analysis for the three axes yields

$$E = 110 d^{-4.7000}, \quad \text{with } r = 0.9932.$$

This is an indication of an extremely fast decrease of tritium release with distance from the source (GS-150). This indicates further that water vapor emanation at the soil-atmosphere interface decreases faster with distance from the source than does the tritium dispersion in the soil, where the distribution behaves as a negative log function of distance. Further work is in progress to correlate tritium emanation to atmospheric and pedological properties of the GS-150 environment, especially including thermal characteristics of the tuff.

The thermal diffusivity ( $D$ ) of the tuff at GS-150 was derived *in situ* from the measurements of daily temperature fluctuations ( $\Delta T$ ) at different depths ( $z$ ) where

$$D = \left( - \frac{\Delta z}{\ln(\Delta T_1/\Delta T_2)} \right)^2 \frac{\pi}{86400\text{s}}$$

averaged consistently  $8 \cdot 10^{-7} \text{ m}^2 \text{ s}^{-1}$  during an extremely dry summer period, which kept the soil moisture content low, resulting in a low specific heat by volume leading to a higher thermal diffusivity. Representative tuff debris was hauled to the laboratory, where the density was accurately established as being  $1.395 \cdot 10^3 \text{ kg m}^{-3}$ .

The specific heat ( $C_s$ ) of the tuff was established in the laboratory using the standard method available for that purpose. A correction, obtained graphically, was used to correct for the thermal leakage of the thermally insulated container that was used as a calorimeter. The test was repeated four times and averaged  $C_s \text{ dry} = 866 \text{ J kg}^{-1} \text{ K}^{-1}$  or a heat capacity  $C_v = 1.208 \cdot 10^6 \text{ J m}^{-3} \text{ K}^{-1}$ . Since the Moisture Ratio by Volume *in situ* turned out to be 0.04, the actual heat capacity of the tuff under consideration is  $C_{v,0.04} = 1.375 \cdot 10^6 \text{ J m}^{-3} \text{ K}^{-1}$ , with a standard deviation of  $2.8 \cdot 10^4 \text{ J m}^{-3} \text{ K}^{-1}$ . The thermal conductivity,  $\lambda$ , was estimated at  $C_{v,0.04} D = 1.1 \text{ W m}^{-1} \text{ K}^{-1}$ .

The above characteristics will help in determining the influence of the vapor gradient in the tuff on tritiated water emanation. Efforts are continuing to monitor temperature, heat flow, and water content at several depths, as well as atmospheric conditions capable of influencing tritium emanation. Relevant tritium elution data gathered so far are listed in Table XI. As one can readily observe, a seasonal pattern seems to emerge, with a peak of tritium release occurring in September. No detailed analysis has been made yet as the data base is far from complete, but the accumulated data would lead one to believe that the maximum releases of tritiated water occur when the vapor pressure within the shaft is driven to its maximum values, while the minimum releases of tritiated water occur when the vapor pressure within the shaft reaches a minimum. It seems evident that the maximum and minimum pressures within the shaft occur when temperatures below the surface reach a maximum or a minimum, respectively.

In conclusion, it should be pointed out that measurements of tritium emanation, taken in comparable locations and in the same seasonal period, yield results that form a good basis for comparison.

- (1) Measurements taken on top of an assumed source of HTO over Pit 1 average  $0.2 \text{ Bq m}^{-2} \text{ s}^{-1}$ .
- (2) In February, at a point 6 m removed from both shafts 50 and 59, a release of  $0.82 \text{ Bq m}^{-2} \text{ s}^{-1}$  was measured.
- (3) By the end of December 1979, along the B axis originating from GS-150, the regression formula  $E = 104 d^{-4.405}$  then obtained yielded  $0.11 \text{ Bq m}^{-2} \text{ s}^{-1}$  at 4.7 m from the shaft, a result that seems

TABLE XI

ACTIVITY AND FLUX OF TRITIATED WATER AT THE SOIL-  
ATMOSPHERE INTERFACE 4.7 m FROM THE CENTER OF GS-150

Date	HTO Concentration		Flux	
	$10^6 \text{ Bq m}^{-3}$	$\mu\text{Ci}/\ell$	$\text{Bq m}^{-2} \text{ s}^{-1}$	$\mu\text{Ci m}^{-2} \text{ day}^{-1}$
28 May 1980	79	2.13	0.58	1.35
4 June 1980	216	5.83	1.61	3.77
11 June 1980	293	7.92	2.00	4.67
18 June 1980	436	11.79	4.26	9.96
25 June 1980	496	13.40	4.47	10.45
2 July 1980	415	11.21	2.60	6.07
9 July 1980	284	7.68	1.63	3.81
16 July 1980	692	18.70	3.15	7.35
23 July 1980	688	18.60	2.62	6.11
30 July 1980	784	21.20	2.98	6.97
6 Aug. 1980	773	20.90	3.60	8.41
13 Aug. 1980	276	7.46	5.48	12.79
20 Aug. 1980	356	9.63	4.89	11.42
27 Aug. 1980	334	9.04	3.78	8.83
3 Sept. 1980	1088	29.40	9.62	22.47
10 Sept. 1980	350	9.45	4.13	9.65
17 Sept. 1980	518	14.00	5.54	12.94
24 Sept. 1980	607	16.40	5.67	13.25
1 Oct. 1980	492	13.30	4.15	9.70
8 Oct. 1980	470	12.70	2.41	5.64
15 Oct. 1980	205	5.54	1.21	2.83
22 Oct. 1980	168	4.55	1.21	2.83
29 Oct. 1980	112	3.03	0.43	1.01
5 Nov. 1980	138	3.73	0.95	2.21
12 Nov. 1980	128	3.46	0.72	1.65
19 Nov. 1980	135	3.64	0.60	1.41
3 Dec. 1980	89	2.40	0.43	1.00
17 Dec. 1980	28	0.75	0.29	0.67
23 Dec. 1980	26	0.69	0.22	0.51
30 Dec. 1980	19	0.50	0.14	0.32
7 Jan. 1981	21	0.57	0.12	0.28
14 Jan. 1981	20	0.5	0.11	0.25
21 Jan. 1981	40	1.08	0.16	0.38
28 Jan. 1981	46	1.25	0.13	0.31
4 Feb. 1981	55	1.49	0.15	0.36
11 Feb. 1981	63	1.70	0.24	0.55
18 Feb. 1981	75	2.03	0.41	0.96
25 Feb. 1981	126	3.40	0.46	1.07

to be quite compatible with actual measurements made by the end of December of the following year, when at 4.7 m from the shaft the emanation was  $0.14 \text{ Bq m}^{-2} \text{ s}^{-1}$ .

Provided the *rate* of fall of tritium emanation with distance from the source remains the same throughout the seasons, the regression equation, during the period of maximum tritium release, is expected to adopt the form  $E_{\text{max}} = 9095 \text{ d}^{-4.405}$ . High release rates around the end of summer and beginning of fall are expected if the observations follow a seasonal pattern. Air concentrations in 1980 that are partly influenced by soil releases (absolute humidity, wind speed, and atmospheric convection will play an important role) also show a maximum during the warmer months and an overall minimum during the month of December.

At 4.7 m from the shaft center (GS-150), the flow of tritiated water averages  $2.19 \text{ Bq m}^{-2} \text{ s}^{-1}$  ( $5.12 \text{ } \mu\text{Ci m}^{-2} \text{ day}^{-1}$ ) with the standard deviation =  $2.20 \text{ Bq m}^{-2} \text{ s}^{-1}$  ( $5.17 \text{ } \mu\text{Ci m}^{-2} \text{ day}^{-1}$ ) at the soil surface. These measurements were taken during the 9 months preceding 25 March 1980.

## IX. STRATIGRAPHIC CONTROLS ON FLOW

The study of the influence of sequential layers of tuff on moisture retention revolved mainly around the influence of related density differences on moisture retention. Densities and moisture contents were measured with nuclear probes that were lowered into monitoring holes. The density and moisture measurements obtained at each depth were then compared. A search for a cause and effect relationship between density and moisture content was subsequently performed through regression analysis.

After subtracting the measured moisture reading from the measured (wet) density, a regression analysis was run on 460 readings using the obtained dry density as the independent variable and the moisture ratio by volume as the dependent variable. The dry density was taken as the independent variable because it is obvious that some correlation would have to exist between the wet density and the moisture present because the moisture would necessarily increase the density measurement.

The dependence of the moisture ratio by volume (MRV) on the density (d) turned out to be

$$\text{MRV} = 0.0210 + 0.0809 d \text{ with } r^2 = 0.0157,$$

indicating that 1.57% of the variation in MRV was associated with d!

More interesting is the fact that the equation shows a *slight* direct relationship between MRV and density, which is in direct contradiction with the observation made on page 52 in "Technical Reports Series No. 112, 1970" from the International Atomic Energy Agency, Vienna. Most authors fail to recognize an effect of soil density on soil moisture measurement in the normal soil density range and our findings can only support that view because of

- (1) a low coefficient of determination between MRV and d.
- (2) The small rate of change of MRV with d (an increase of  $100 \text{ kg m}^{-3}$  in density would mean an *increase* of 0.008 in the MRV).
- (3) The proponents of a possible interaction between MRV and d indicate it would be an *inverse* correlation. The data presented do not give an indication of how strong (or weak) that correlation is supposed to be. The lack of interference of d in the moisture readings could only result in a narrowing of the confidence limits obtained when the moisture ratio is expressed as a function of the count ratio. Estimates of these confidence limits have been published and widely discussed (see Abeele, October 1979).

Subsequent logging by the US Geological Survey (USGS) showed that the actual monitoring hole diameter was, in some cases, not uniform, causing discrepancies in the moisture evaluation because of the application of the inappropriate calibration formula for that particular depth. An important parameter had consequently been overlooked. To remedy that, the regression analysis was repeated for the monitoring holes with irregular diameters. The analysis was applied over the depth range where the actual measured diameter matched the nominal diameter used in calibrating the neutron moisture probe readings. This obviously led to the elimination of the unwanted parameter. Somewhat different degrees of correlation were obtained for monitoring holes CS2-1, CS5-1, and CS6-1.

CS2-1	$\text{MRV} = -0.17 + 0.23d$	$r^2 = 0.17$
CS5-1	$\text{MRV} = 0.06 + 0.00074d$	$r^2 = 0.0019$
CS6-1	$\text{MRV} = 0.05 + 0.07d$	$r^2 = 0.07$

with  $r^2$  being the coefficient of determination.

As can be seen, none of the correlations are significant. (In the case of CS5-1, one would have to try hard to obtain as bad a correlation between two columns of numbers chosen completely at random.) Moreover, in every case, the equations show again a slight *direct* relationship between MRV and density. The obvious conclusion of the study is that, in the range of tuff densities considered, there is no cause and effect relationship between density and moisture content.

## X. RADIONUCLIDE TRANSPORT STUDIES

### A. Downward Migration Through Leaching

Samples were collected along horizontal cores beneath Pit 3 in Area G for radiochemical analysis (Purtymun et al., 1978). For this purpose, a drill pad was constructed in a small canyon east of the pit from where five horizontal holes were cored under the pit. The study was performed in an attempt to detect possible migration of radionuclides from the waste pit into the tuff immediately underlying it. Core samples were analyzed for gross alpha, gross beta,  $^{90}\text{Sr}$ ,  $^{238,239,240}\text{Pu}$ ,  $^{241}\text{Am}$ ,  $^{137}\text{Cs}$ , and total uranium as contaminants in the waste. Filling of the pit was started 13 years before the core analysis study was begun. The tuff present on location was divided into several stratigraphic units, distinguishable from each other through their chemical and physical properties. Consequently, the natural concentrations of radionuclides vary from unit to unit.

The horizontal core holes were drilled in a fan-shaped array beneath the disposal pit. Samples of tuff beneath the pit and adjacent to it were analyzed for radionuclides known to be present in the pit, as well as for gross alpha and gross beta radiation. The analytical results from samples obtained beneath the pit were then compared statistically with the analytical results from samples obtained beside the pit. The analytical results were also grouped as a function of stratigraphic units.

The analytical results showed conclusively that the man-made radionuclides known to be present in the pit were not present at concentrations above the minimum detection limits in the samples collected beneath the pit. There were no statistically significant differences in gross alpha or gross beta radiation, or in concentrations of naturally occurring radionuclides in samples originating from under the pit compared with the samples obtained adjacent to the pit but pertaining to the same stratigraphic unit. In this context, it should be pointed out that the uranium concentrations varied between stratigraphic units but that the mean concentrations found in specific core samples were statistically undistinguishable from concentrations measured in related outcrops. Variabilities in gross alpha concentrations between units were found to be related to the already observed variability in uranium and other naturally occurring radionuclides.

Many of the waste containers in the pit were undoubtedly ruptured at the time of disposal through compaction by heavy earthmoving equipment. Also, much of the disposed waste, including contaminated soil, was not isolated from its environment. Thus, most of the radionuclides in the pit can be assumed to be available for dissolution and removal by moving soil moisture. The actual rates of dissolution and removal are not known but some must have happened locally in the 13 years that have elapsed since the initial use of the disposal pit. Results show, however, that any local radionuclide movement was restricted to the confines of the pit.

Expected water flow velocities, in the solid and crushed tuff, are known to be on the order of  $10^{-12} \text{ m s}^{-1}$  at the measured low soil moisture contents. This suggests that no migrating solutions would be detectable at depths exceeding a few millimeters beneath the pit. That expectation was not contradicted by the measurements taken in this study. No radionuclides, whose presence can be attributed to migration from the pit, were detected (Purtymun et al., 1980).

### B. Upward Migration via Evapotranspiration

Surface contamination was known to exist in Area C, where the total activity in the top 5 cm of soil was calculated to be approximately  $3 \cdot 10^{10} \text{ Bq}$ . Several hypotheses have been advanced to account for the presence of the surface contamination (Trocki et al., in press).

- (1) The nature of the disposal operations,
- (2) the nature of known nuclear waste retrieval operations,
- (3) burrowing animals,
- (4) possible inadequate pit cover, and/or
- (5) upward migration of radionuclides.

Core samples of several contaminated spots in Area C were analyzed for  $^{238}\text{Pu}$ ,  $^{239}\text{Pu}$ , and  $^{241}\text{Am}$ . Three corings, representative of how the activity was distributed as a function of depth, yielded the following regression equations (A is activity expressed in  $\text{Bq kg}^{-1}$  and d in meters depth).

I.D. No. CPS-16

$$^{238}\text{Pu}: A = 1.04 \cdot 10^{-3} d^{-6}$$

$$^{239}\text{Pu}: A = 2.04 \cdot 10 d^{-2.85}$$

$$^{241}\text{Am}: A = 0.91 d^{-4.3}$$

I.D. No. CPS-18

$$^{238}\text{Pu}: A = 3.7 \cdot 10^{-3} d^{-4}$$

$$^{239}\text{Pu}: A = 1.37 d^{-3.64}$$

$$^{241}\text{Am}: A = 2.59 \cdot 10^{-2} d^{-5}$$

I.D. No. CPS-11

$$^{241}\text{Am}: A = 0.74 d^{-2.07}$$

The above numbers are the identification of some of the contaminated spots under scrutiny in Area C.

These equations demonstrate a strong decrease of activity with depth. This strengthens the notion of surface spill as the source and no "upwelling" from the pit because of transport mechanisms involving evapotranspiration. The lack of uniformity, as far as the shape of the corresponding decreased activity curves is concerned, cannot be explained based on available information.

The decreasing activity with depth can only be a result of a slow leaching of radionuclides downward from their original surface spill location.

## XI. SHEAR IN WET COHESIONLESS SOILS AND CRUSHED TUFF

Negative stress induced by capillary tension can be at the origin of increased soil shear strength. Capillary tension is the driving force that enables moist sand to maintain a molded or cut shape. Thin water films with small meniscus radii develop high-tensile stresses in the moisture wedges that hold soil particles in rigid contact. Fine sands and silts within the zone of capillary rise and fringe above a water table owe their strength to capillary tension and the resulting effective stresses in the granular structure. A point of maximum stress exists as a function of moisture content for a particular soil. Any drying or wetting away from that optimum moisture content will mean a decrease in maximum shear strength. The components of shear strength are friction and cohesion. The friction component is primarily affected by physical factors, while physiochemical factors affect the cohesion component. Cohesion is dependent on the attractive forces at work in clay-particle interactions. Water plays an important role in determining the magnitude of the cohesion component because it affects the distance between soil particles and, consequently, the attractive forces associated with air-water menisci (Baver et al., 1972). Excavation failures can sometimes be traced to a departure from a higher shear strength that existed when excavation was first begun.

A vane shear test was performed on soils and crushed tuff originating from the GS-150 area. As can be seen from Tables XII and XIII and Figs. 20 and 21, the decrease in strength caused by further wetting is much more drastic than that induced by eventual drying. For any granular material, the strength characteristics will depend heavily on the dry unit mass to which it is compacted. A higher dry unit mass

TABLE XII

VANE SHEAR TEST ON SOIL

Moisture Content by Mass (%)	Shear Strength (kPa)
2	7.25
8	7.2
12	7.6
16	8.0
20	6.0
24	3.0
26	0

TABLE XIII

VANE SHEAR TEST ON CRUSHED TUFF

Moisture Content by Mass (%)	Shear Strength (kPa)
1	1.0
10	5.8
12	8.2
14	12.8
16	14.0
18	14.2
20	14.6
22	16.2
24	16.2
26	10.2
28	0.0

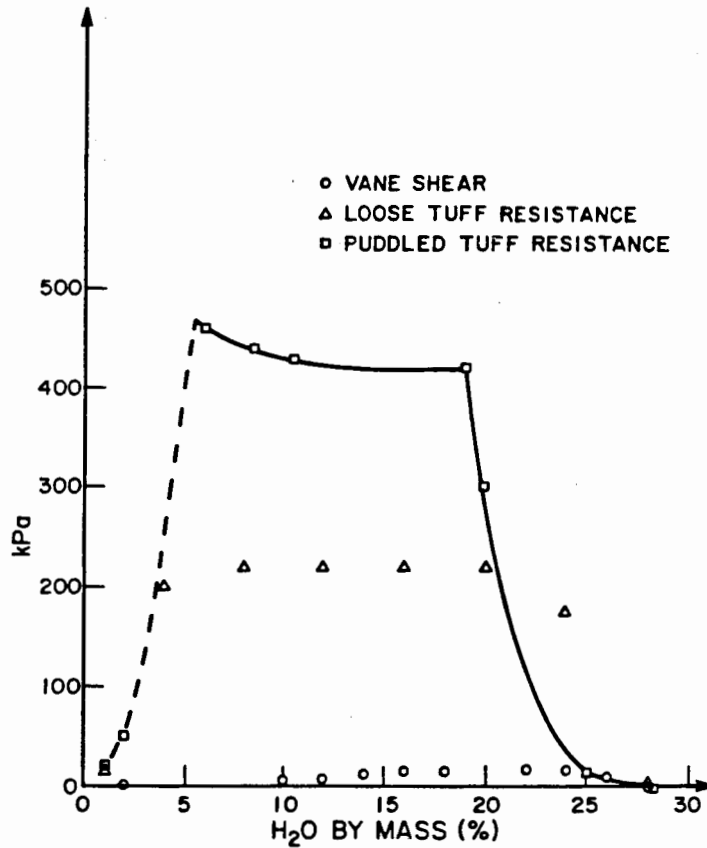


Fig. 20. Resistance tests on tuff.

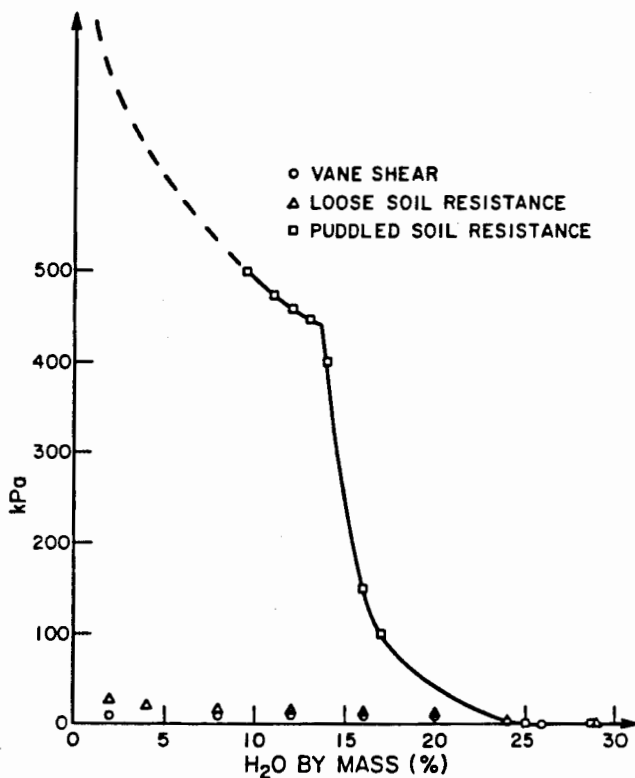


Fig. 21. Resistance tests on soil.

will correspond to a higher shear strength, all other parameters being equal. Changes in dry unit mass and shear strength are both influenced by the same independent variable, moisture content. A plot of dry density vs moisture content will indicate that compaction at any given energy level becomes more efficient as the moisture content increases toward an optimum moisture level beyond which the efficiency decreases.

The least expensive way to improve soil stabilization is precisely through compaction. Soil stabilization in turn means the improvement of several physical properties which, among other things, determine the shear strength of that soil. Besides an increase in shear strength, the other physical properties of a soil improved by compaction are the related increase in dry density and subsequent decreases in compressibility, permeability, and shrinkage (this last property mainly applicable to the montmorillonite clay that can be found on-site). As can be seen, adequate compaction of the pit overburden will improve several desirable properties important for good nuclear waste management.

The resistance to the penetration of a probing instrument is an integrated index of compaction, moisture content, texture, and type of material involved (crushed tuff, various clays, sand, etc.). As a penetrometer enters the soil, it will encounter resistance to compression, some friction between soil and metal and the shear resistance of the soil, which, as described above, involves both internal friction and cohesion (Baver et al., 1972).

The probe used in this study is a flat-bottom one. The tests show that soil moisture is a dominant factor influencing penetration resistance. There is a rapid decrease in resistance above 20% moisture by weight in crushed tuff and above 0% in the corresponding soil (Tables XIV and XV and Figs. 20 and 21). In tuff and soil the resistance to penetration at a moisture content of 16% by mass increases with depth of penetration.

TABLE XIV

RESISTANCE TO PENETRATION  
IN TUFF

Moisture Content by Mass (%)	Resistance (kPa)
1	15
4	200
8	220
12	220
16	220
20	220
24	175
28	0

TABLE XV

RESISTANCE TO PENETRATION  
IN SOIL

Moisture Content by Mass (%)	Resistance (kPa)
2	27
4	20
8	15
12	12
16	9
20	6
24	3
28	1

In tuff, the resistance to penetration,  $R$ , as a function of penetration depth,  $p$ , can be expressed as

$$R = 46p^{0.871} \quad r^2 = 0.998$$

while in soil, the penetration resistance can be expressed as

$$R = 1.684p^{0.925} \quad r^2 = 0.997$$

where  $R$  is expressed in kPa and  $p$  in mm.

The above results were obtained through regression analysis and in both cases the best results were obtained by adaptation of a power curve fit. As can be noticed, both expressions are nearly linear, which indicates that resistance to penetration increases *almost* proportionally with the penetration depth. If resistance to penetration is mainly a function of shear and compression resistance, it is fairly obvious from Figs. 20 and 21 that, for both tuff and soils, compression resistance is the most important component of the resistance to penetration and also the most sensitive to moisture content.

Application of similar compacting pressures on both crushed tuff and soil was at the origin of one notorious behavioral difference. The maintenance of that pressure caused practically no subsidence in the tuff as the moisture content was increased, while subsidence in the soil reached a high of 6%. This last phenomenon is well known to occur in soils, undoubtedly as a result of the enhanced ease of orientation of particles above the plastic limit. The soil in question, a very fine sandy loam, contains clay that has a platy or sheet-like structure. Because particle orientation is one of the major causes of subsidence (*or increased density*) during compression and because water is acting as a lubricant to facilitate such reorientation, it is to be expected that the soil under study will increase in density as the moisture content is increased. The near absence of that phenomenon in the crushed tuff indicates the absence of a platy structure and consequent minimum reorientation through lubrication (spherical particles do not possess a preferential orientation).

It should be noticed that in all of the above tests, the moisture was progressively *added* to loose, dry soil or tuff.

Tables XVI and XVII show how the resistance to penetration changes as a function of moisture after puddling and subsequent desiccation. It can be seen that the resistance to penetration reaches higher values using puddled materials. Drying of puddled soils produces maximum contact between particles, which causes high cohesion and strength due to interparticle attraction. Cohesion increases with a decrease in particle size distribution. Consequently, the point of maximum cohesion will increase with the

TABLE XVI

RESISTANCE TO PENETRATION  
IN TUFF AFTER PUDDLING

Percent H <sub>2</sub> O	kPa
28	0
25	15
20	300
19	420
10.5	430
8.5	440
6.5	450
6	460
2	50
1	15

TABLE XVII

RESISTANCE TO PENETRATION  
IN SOIL AFTER PUDDLING

Percent H <sub>2</sub> O	kPa
28	1
25	1
17	100
16	150
14	400
13	450
12	460
11	475
9.5	500
2	> 500
1	>> 500

clay content of the materials under study. It is clear from Figs. 20 and 21 that the amount of cohesive soil is greater in soils than in crushed tuff. As a matter of fact, the resistance to penetration in soils increases rapidly beyond the measurement capabilities of the penetrometer in use. The dashed line in Fig. 21 indicates the suggested shape of the penetration resistance curve of puddled soil vs moisture content. Furthermore, it needs to be pointed out that the equation, expressing the resistance to penetration as a function of penetration depth, is not valid for dried puddled soils. Once the resistance of the "crust" is overcome, continued penetration occurs without any further increase in pressure. At very low moisture content (2%), the attraction between particles breaks down completely in tuff, while it continues to increase in soils, reaching its maximum at the lowest moisture content while tuff regains its complete loose state at 1% moisture content.

Just as the shear strength of crushed tuff, at a given moisture content, is very much a function of its dry density, so is the strength of undisturbed tuff equally dependent on its density (Purtymun et al., 1965). For several sites in the Los Alamos area, the influence of density (D) on resistance to crushing (RC) can be expressed as

$$RC = -383 + 51.72 \ln D$$

where the resistance to crushing is expressed in MPa and the bulk density in kg m<sup>-3</sup>.

## ACKNOWLEDGMENTS

Thanks are due to W. Herrera for computer plotting of the figures, to E. Trujillo and W. Herrera for sample collection, and to W. D. Purtymun for his pertinent advice.

## REFERENCES

- W. V. Abeele, "Future Credible Precipitation Occurrences in Los Alamos, New Mexico," Los Alamos Scientific Laboratory report LA-8523-MS (September 1980).
- W. V. Abeele, "Determination of Hydraulic Conductivity in Crushed Bandelier Tuff," Los Alamos Scientific Laboratory report LA-8147-MS (November 1979).

W. V. Abeele, "The Influence of Access Hole Parameters on Neutron Moisture Probe Readings," Los Alamos Scientific Laboratory report LA-8094-MS (October 1979).

J. H. Abrahams, Jr., "Physical Properties of and Movement of Water in the Bandelier Tuff, Los Alamos and Santa Fe Counties, N.M.," US Dept. of the Interior Geological Survey, Albuquerque, New Mexico (January 1963).

J. H. Abrahams, Jr., J. E. Weir, Jr., and W. D. Purtymun, "Distribution of Moisture in Soil and Near-Surface Tuff on the Pajarito Plateau, Los Alamos County, N.M., U.S.G.S. Professional Paper 424D," Geological Research (1961).

R. A. Bailey, R. L. Smith, and C. S. Ross, "Stratigraphic Nomenclature of Volcanic Rocks in the Jemez Mountains, New Mexico," US Geol. Survey Bull. 1474 p. (1969).

L. D. Baver, W. H. Gardner, and W. R. Gardner, *Soil Physics* (John Wiley & Sons, New York, 1972), pp. 74-125.

G. S. Campbell, "A Simple Method for Determining Unsaturated Conductivity from Moisture Retention Data," *Soil Sci.* 117:311-314 (1974).

DOE/EIS-0018, "Final Environmental Impact Statement - Los Alamos Scientific Laboratory Site, Los Alamos, New Mexico," US Department of Energy (December 1979).

R. L. Griggs, "Geology and Ground Water, Los Alamos Area, New Mexico," U. S. Geol. Survey Water Supply Paper, 1753 p. (1964).

International Atomic Energy Agency, "Neutron Moisture Gauges," Technical Report Series No. 112, Vienna (1970).

R. D. Jackson, R. J. Reginato, and C. H. M. Van Bavel, "Comparison of Measured and Calculated Hydraulic Conductivities of Unsaturated Soils," *Water Resources Rev.* 1, pp. 375-380 (1965).

A. Klute, "Water Diffusivity. Methods of Soil Analyses," *Amer. Soc. of Agronomy*, pp. 262-272 (1965).

R. J. Kunze, G. Vchara, and K. Graham, "Factors Important in the Calculation of Hydraulic Conductivity," *Soil Sci. Soc. Amer. Proc.* 32:760-765 (1968).

E. E. Miller and D. E. Elrick, "Dynamic Determination of Capillary Conductivity Extended for Nonnegligible Membrane Impedance," *Soil Sci. Soc. Amer. Proc.* 22:483-486 (1958).

R. J. Millington and J. P. Quirk, "Permeability of Porous Solids," *Trans. Faraday Soc.* 57:1200-1207 (1961).

W. D. Purtymun, "Underground Movement of Tritium from Solid Waste Storage Shafts," Los Alamos Scientific Laboratory report LA-5286-MS (May 1973).

W. D. Purtymun, M. L. Wheeler, and M. A. Rogers, "Geologic Description of Cores from Holes P-3 MH-1 through P-3 MH-5, Area G, Technical Area 54," Los Alamos Scientific Laboratory report LA-7308-MS (May 1978).

W. D. Purtymun and W. R. Kennedy, "Geology and Hydrology of Mesita del Buey," Los Alamos Scientific Laboratory report LA-4660 (May 1971).

W. D. Purtymun and W. E. Kennedy, "Distribution of Moisture and Radioactivity in Soil and Tuff at the Contaminated Waste-Pit Near Technical Area 21, Los Alamos, N.M.," US Geol. Survey Open File report (1966).

W. D. Purtymun and F. C. Koopman, "Physical Characteristics of the Tshirege Member of the Bandelier Tuff with Reference to Use as a Building and Ornamental Stone," US Geol. Survey Open File report, Albuquerque, N.M. (1965).

W. D. Purtymun, M. A. Rogers, and M. L. Wheeler, "Radiochemical Analyses of Samples from Beneath a Solid Radioactive Waste Disposal Pit at Los Alamos, N.M.," Los Alamos Scientific Laboratory report LA-8422-MS (June 1980).

P. E. Rijtema, "Calculation of Capillary Conductivity from Pressure Plate Outflow Data with Nonnegligible Membrane," Neth. J. Agr. Sci. 7:209-215 (1959).

M. A. Rogers, "History and Environmental Setting of LASL Near-Surface Land Disposal Facilities for Radioactive Wastes," Los Alamos Scientific Laboratory report LA-6848-MS (June 1977).

E. Schulman, "Tree-Ring Indices of Rainfall, Temperature, and River Flow," Compendium of Meteorology (American Meteorological Society, Boston, 1951), pp. 1024-1029. See also Tree-Ring Bulletin 18, 10-18 (1952).

R. L. Smith, R. A. Bailey, and C. S. Ross, "Geologic Map of the Jemez Mountains, New Mexico," US Geol. Survey Misc. Geol. Investigation Map I - 571 (1970).

L. K. Trocki and W. V. Abeele, "Radioactivity Inventory of the Surface of Closed Waste Disposal Area C," Los Alamos National Laboratory report (in press).

M. L. Wheeler, W. J. Smith, and A. F. Gallegos, "A Preliminary Evaluation of the Potential for Plutonium Release from Burial Grounds at Los Alamos Scientific Laboratory," Los Alamos Scientific Laboratory report LA-6694-MS (February 1977).

M. L. Wheeler and J. L. Warren, "Tritium Containment After Burial of Contaminated Solid Waste," Proceedings of 23rd Conference on Remote Systems Technology (1975).

## APPENDIX

### SUMMARY OF DEPTH RANGES AND MEASUREMENT DATES FOR MONITORING HOLES - 1980

Number		Jan.	Feb.	Mar.	April	May	June
CP2180	Start	ND	00.50	00.50	00.50	00.50	00.50
	End		31.50	32.00	29.50	29.50	31.00
CP5180	Start	ND	00.50	00.50	00.50	00.50	ND
	End		29.50	27.50	27.50	27.50	
CP6180	Start	ND	00.50	00.50	00.50	00.50	00.50
	End		23.50	24.00	23.00	23.00	23.50
CS9980	Start	ND	00.50	00.50	00.50	00.50	00.50
	End		30.00	31.00	29.50	29.50	30.50
FP1180	Start	ND	00.50	00.50	00.50	00.50	ND
	End		21.00	21.00	21.00	21.00	21.00
GP1180	Start	ND	00.50	00.50	00.50	00.50	00.50
	End		5.50	5.50	5.00	5.00	5.00
GP1280	Start	ND	00.50	00.50	00.50	00.50	00.50
	End		3.50	3.50	3.50	3.50	3.00
GP2680	Start	ND	00.50	00.50	00.50	00.50	00.50
	End		33.00	31.50	31.00	31.00	31.50
GP7280	Start	ND	NE	9.00	9.00	9.00	9.00
	End			24.00	22.50	22.50	23.50
GP7380	Start	ND	9.00	9.00	9.00	9.00	9.00
	End		22.00	22.00	20.00	20.00	21.50
GS50380	Start	00.50	00.50	00.50	00.50	00.50	00.50
	End	11.50	12.00	12.00	11.50	11.50	12.00
GS50580	Start	00.50	00.50	00.50	00.50	00.50	00.50
	End	14.00	14.50	14.50	14.00	14.00	14.00
TA52180	Start	ND	00.50	00.50	00.50	00.50	00.50
	End		33.00	32.00	30.00	30.00	31.00
TA5180	Start	ND	00.50	00.50	00.50	00.50	ND
	End		33.00	31.50	30.00	30.00	(Lost Probe)

ND = No Data

NE = Data Not Entered

SUMMARY OF DEPTH RANGES AND MEASUREMENT DATES  
FOR MONITORING HOLES - 1979

Number	Jan.	Feb.	Mar.	April	May	June	July	Aug.	Sept.	Oct.	Nov.	Dec.
GS50319												
Start	ND	ND	0.5	ND	0.5	0.5	0.5	0.5	0.5	0.5	0.5	0.5
End			11.5		11.5	12.0	11.5	12.0	12.0	12.5	11.5	12.0
GS50579												
Start	0.5	NM	0.5	ND	0.5	0.5	0.5	0.5	0.5	0.5	0.5	0.5
End	14.0		14.0		14.0	14.0	14.0	15.0	14.0	15.0	15.0	14.5
GR1179												
Start	0.5	0.5	0.5	ND	0.5	0.5	0.5	0.5	0.5	0.5	0.5	0.5
End	5.0	5.0	5.0		5.0	5.5	5.0	5.0	5.0	5.5	5.0	5.5
GP1279												
Start	0.5	0.5	0.5	ND	0.5	0.5	0.5	0.5	0.5	0.5	0.5	0.5
End	3.5	3.5	3.5		3.5	4.0	3.5	4.0	3.5	4.0	3.5	4.0
GP7279												
Start	9.0	9.0	9.0		9.0	9.0	9.0	9.0	9.0	9.0	9.0	ND
End	22.5	24.5	22.5		23.0	23.5	23.0	23.5	23.5	26.0	23.5	
GP7379												
Start	9.0	9.0	9.0	ND	9.0	9.0	9.0	9.0	9.0	9.0	9.0	ND
End	20.0	21.0	20.0		20.5	22.5	20.5	21.5	20.5	22.5	20.5	
CP2179												
Start	0.5	0.5	0.5	ND	0.5	0.5	0.5	0.5	0.5	0.5	0.10	ND
End	29.5	25.5	29.5		29.5	29.5	29.5	26.0	29.5	32.5	29.5	
CP6179												
Start	0.5	0.5	0.5	ND	0.5	0.5	0.5	0.5	0.5	0.5	0.10	ND
End	24.0	30.0	24.50		24.0	22.0	22.5	23.5	28.0	24.5	23.0	
CS99179												
Start	0.50	0.50	0.50	ND	0.50	0.50	0.5	0.5	0.5		0.5	ND
End	30.50	20.00	30.50	ND	30.50	29.50	30.5	28.5	30.0	31.0	30.0	
CP5179												
Start	0.5	0.5	ND	ND	0.5	0.5	0.5	0.5	0.5	0.5	0.10	ND
End	27.5	30.5			27.5	29.0	27.5	28.5	28.0	29.5	27.5	
CP5179												
Start	0.5	0.5	0.5		0.5	0.5	0.5	0.5	0.5	0.5	0.10	ND
End	30.5	28.0	30.5		30.5	29.5	30.5	28.5	28.0	29.5	27.5	
FP1179												
Start											0.5	ND
End											21.0	
GP26179												
Start											ND	0.5
End												33.0
TA52179												
Start											ND	0.5
End												33.0
TA5179												
Start											0.5	ND
End											33.0	
CP5179												
Start	0.5	0.5	ND	ND	0.5	0.5	0.5	0.5	0.5	0.5	0.5	0.5
End	27.5	30.5	ND	ND	27.5	29.0	27.5	28.5	28.0	29.5	27.5	
CP5179												
Start	0.5	0.5	0.5		0.5	0.5	0.5	0.5	0.5	0.5	0.10	ND
End	30.5	28.0	30.5	30.5	29.5		30.5	28.5	28.0	29.5	27.5	
FP179												
Start											0.5	ND
End											21.0	

SUMMARY OF DEPTH RANGES AND MEASUREMENT DATES  
FOR MONITORING HOLES - 1976, Continued

Number	Jan.	Feb.	Mar.	April	May	June	July	Aug.	Sept.	Oct.	Nov.	Dec.
GP26179												
Start											ND	0.5
End												33.0
TA52179												
Start											ND	0.5
End												33.0
TA5179												
Start											0.5	ND
End											33.0	

SUMMARY OF DEPTH RANGES AND MEASUREMENT DATES  
FOR MONITORING HOLES - 1978

Number	Jan.	Feb.	Mar.	April	May	June	July	Aug.	Sept.	Oct.	Nov.	Dec.
CP2178												
Start							0.5	0.5		0.5	0.5	
End							29.5	29.5		29.5	31.0	
CPS178												
Start								0.5			0.5	0.5
End								31.0			31.5	30.5
GS50178												
Start	0.91	0.91	0.5	0.5	0.5	0.5	0.5	0.5	0.5	0.5	0.5	0.5
End	14.02	12.80	13.5	13.0	13.5	13.5	13.0	13.5	13.0	13.5	13.5	13.0
GS50378												
Start	0.5	0.5	0.5	0.5	0.5	0.5	0.5	0.5	0.5	0.5	0.5	0.5
End	11.0	11.0	12.0	12.0	12.5	11.5	11.5	12.0	11.5	11.5	12.0	11.5
GS50578												
Start	0.91	0.91	0.5	0.5	0.5	0.5	0.5	0.5	0.5	0.5	0.5	0.5
End	14.33	14.02	13.50	13.5	14.0	14.0	13.0	14.0	14.0	14.0	14.5	13.0
GA1178												
Start	0.61	0.61	0.5	0.5	0.5	0.5	0.5	0.5	0.5	0.5	0.5	0.5
End	5.49	5.49	5.00	5.0	5.0	5.0	5.0	5.0	5.0	5.0	5.0	5.0
GP1278												
Start	0.61	0.61	0.5	0.5	0.5	0.5	0.5	0.5	0.5	0.5	0.5	0.5
End	3.96	3.96	3.50	3.5	3.5	3.5	3.0	3.5	3.5	3.5	4.0	3.5
GP7178												
Start	8.53	8.53	9.0	9.0	9.0	9.0	9.0	9.0	9.0	9.0	9.0	9.0
End	24.68	24.07	23.0	23.0	23.0	24.0	25.0	23.5	23.0	23.0	23.5	23.0
GP7378												
Start	8.53	8.53	9.0	9.0	9.0	9.0	9.0	9.0	9.0	9.0	9.0	9.0
End	21.33	21.03	14.0	20.0	21.5	21.5	20.0	20.0	20.0	20.0	21.0	20.0
GP6178												
Start								0.5		0.5	0.5	0.5
End								24.0		24.0	25.5	24.0
GP5178												
Start								0.5	0.5	0.5	0.5	0.5
End								29.0	27.5	27.5	28.0	27.5

**SUMMARY OF DEPTH RANGES AND MEASUREMENT DATES  
FOR MONITORING HOLES - 1977**

Number	Jan.	Feb.	Mar.	April	May	June	July	Aug.	Sept.	Oct.	Nov.	Dec.
<b>GS50177</b>												
Start	2.13	2.13	2.43	2.13	2.43	2.13	2.13	2.13	0.91	1.21	1.52	1.21
End	11.58	9.45	11.58	8.53	14.62	9.45	9.14	14.33	14.02	14.02	14.02	13.72
<b>GS50377</b>												
Start	1.82	1.82	2.13	2.43	2.43	2.13	2.13	1.82	1.82	1.21	1.21	0.91
End	13.72	12.80	12.80	11.58	13.41	13.11	13.41	14.02	13.41	12.50	12.50	12.19
<b>GS50577</b>												
Start	1.82	1.82	2.13	2.13	1.82	2.13	2.13	1.82	1.82	1.21	1.21	1.21
End	9.45	9.45	9.75	9.14	13.72	9.45	14.33	14.64	14.63	13.41	14.02	14.02
<b>GP177</b>												
Start	1.82	1.52	1.21	1.21	1.52	2.13	1.82		1.21	1.21	1.21	1.21
End	5.49	5.49	4.57	5.18	5.49	5.49	5.79		5.49	5.49	5.79	5.49
<b>GP1277</b>												
Start	1.82	1.52	1.52	1.21	1.52	1.52			1.52	1.21	1.21	1.21
End	4.27	4.27	4.27	3.96	4.27	4.27			4.27	4.27	4.27	4.27
<b>GP7177</b>												
Start	8.53	8.53	8.53		8.53	8.53	8.53		8.53	8.53	8.53	8.53
End	24.38	14.33	14.02		24.07	14.02	14.94		24.07	22.86	22.86	22.86
<b>GP7377</b>												
Start	8.53	8.53	8.53		8.53	8.53	8.53		8.53	8.53	8.53	8.53
End	20.72	13.41	14.33		21.03	14.02	13.41		21.03	21.03	20.11	19.81

**SUMMARY OF DEPTH RANGES AND MEASUREMENT DATES  
FOR MONITORING HOLES - 1976**

Number	Jan.	Feb.	Mar.	April	May	June	July	Aug.	Sept.	Oct.	Nov.	Dec.
<b>GS0176</b>												
Start	1.52		1.52				1.52	1.52				1.52
End	13.41		9.75				7.62	8.53				7.92
<b>GS50276</b>												
Start	1.52		1.52				1.52	1.52				1.52
End	13.71		10.06				10.06	10.06				10.06
<b>GS50376</b>												
Start	1.52		1.52				1.52	1.52				1.52
End	13.41		10.06				9.75	9.45				10.06
<b>GS50476</b>												
Start	1.52		1.52				1.52	1.52				1.52
End	12.50		8.84				8.23	8.84				8.84
<b>GS50576</b>												
Start	1.52		1.52				1.52	1.52				1.52
End	13.41		10.06				7.92	7.92				8.23
<b>GS50676</b>												
Start	1.52		1.52				1.52	1.52				1.52
End	13.11		8.53				7.62	7.92				9.14
<b>GP1176</b>												
Start	0.91						0.91	0.91				0.91
End	4.88						4.88	4.88				4.88

**SUMMARY OF DEPTH RANGES AND MEASUREMENT DATES  
FOR MONITORING HOLES - 1979, Continued**

Number	Jan.	Feb.	Mar.	April	May	June	July	Aug.	Sept.	Oct.	Nov.	Dec.
GP1276												
Start	0.91						0.91	0.91				0.91
End	3.66						3.66	3.66				3.66
GP2176												
Start	0.91						0.91	0.91				0.91
End	2.74						3.05	2.74				2.44
GP2276												
Start	0.91						0.91	0.91				0.91
End							1.21	1.21				

**SUMMARY OF DEPTH RANGES AND MEASUREMENT DATES  
FOR MONITORING HOLES - 1975**

Number	Jan.	Feb.	Mar.	April	May	June	July	Aug.	Sept.	Oct.	Nov.	Dec.
GP1175												
Start			0.30									
End				4.55								
GP1275												
Start			0.30									
End			3.30									
GP1175												
Start				0.30				0.30				
End				4.55				4.55				
GP1275												
Start				0.30				0.30				
End				3.94				3.58				

**SUMMARY OF DEPTH RANGES AND MEASUREMENT DATES  
FOR MONITORING HOLES - 1974**

Number	Jan.	Feb.	Mar.	April	May	June	July	Aug.	Sept.	Oct.	Nov.	Dec.
GP1174												
Start	0.30	0.30	0.30	0.30	0.30	0.30	0.30	0.30	0.30	0.30		
End	5.12	4.85	4.85	4.85	5.10	4.24	2.42	5.10	5.10	4.24		
GP1274												
Start	0.30	0.30	0.30	0.30	0.30	0.30	0.30	0.30	0.30	0.30		
End	3.64	3.58	3.64	3.58	3.58	3.58	3.58	3.58	3.58	3.30		
GP2174												
Start		0.30										
End		2.73										
GP2274												
Start		0.30										
End		1.15										
GP2174												
Start			0.30									
End			2.73									
GP2274												
Start			0.30									
End			1.20									